BPC-157 Binding to SH3 Domains and Activation of Src Family Kinases: In Silico Modeling and Fluorescent Fusion Protein Production

STEVEN K SCHLOSSER

cellshotnutrition@gmail.com

Cell Shot Nutrition https://orcid.org/0000-0003-0568-2728

Research Article

Keywords: BPC-157, Src Family Kinases, SH3 Domain, In Silico Docking, Fluorescent BPC-157 Protein, Mechanism of Action

Posted Date: December 5th, 2025

DOI: https://doi.org/10.21203/rs.3.rs-8167242/v2

Additional Declarations: The authors declare potential competing interests as follows: Steven Schlosser is the CEO of Cell Shot Nutrition. This company does not manufacture or market products related to the subject of this manuscript.

BPC-157 Binding to SH3 Domains and Activation of Src Family Kinases: In Silico Modeling and Fluorescent Fusion Protein Production

Steven K. Schlosser[a*] *ORCID: 0000-0003-0568-2728*

[a]Cell Shot Nutrition LLC, 6076 Corte del Cedro, Carlsbad, CA, 92011, USA, cellshotnutrition@gmail.com

*Corresponding Author

Abstract

Body Protection Compound-157 (BPC-157) is a synthetic pentadecapeptide derived from human gastric juice with regenerative and cytoprotective effects reported across diverse tissues. Despite extensive preclinical study, the precise molecular mechanism underlying BPC-157's pleiotropic pro-repair effects remains incompletely understood. A key unresolved question is whether BPC-157 acts through extracellular receptor engagement, via intracellular interactions, or through a combination of both. Drawing on preclinical literature, structural modeling, and in silico docking, I propose that BPC-157 adopts a polyproline II helix that engages the Src homology 3 (SH3) domains of Src family kinases (SFKs; c-Src, Yes, Fyn). This interaction relieves SH3 domain-mediated autoinhibition of SFKs, resulting in focal adhesion kinase (FAK)-extracellular signal-regulated kinase (ERK) and phosphoinositide 3-kinase (PI3K)-protein kinase B (Akt) signaling cascades. To enable future experimental validation, a custom baculovirus encoding an engineered mCherry-BPC157_2 fusion protein was generated and used to transduce *Spodoptera frugiperda* (Sf9) cells. Expression of mCherry-BPC157_2 was validated by fluorescent imaging and confirmed by western blot at the expected molecular weight (~31 kDa). Collectively, this work proposes a novel structural and functional mechanism for BPC-157, provides in silico docking support, and introduces a molecular tool to probe the BPC-157 interactome.

1.0
Introduction

1.1
BPC-157 Pro-Repair Signaling: Biological Effects and Mechanistic Insights

Body Protection Compound-157 (BPC-157) is a synthetic 15-amino-acid peptide (sequence: Gly-Glu-Pro-Pro-Pro-Gly-Lys-Pro-Ala-Asp-Asp-Ala-Gly-Leu-Val), originally derived from a protein fragment found in human gastric juice [*1*]. Over the past three decades, preclinical research has demonstrated its regenerative and cytoprotective effects across diverse tissues [*2,3*]. Despite these promising findings, BPC-157 remains investigational, with regulatory concerns stemming from limited pharmacokinetic data and issues related to peptide purity.

At the cellular level, BPC-157 activates two primary signaling cascades: the focal adhesion kinase (FAK)–extracellular signal-regulated kinase (ERK) pathway and the phosphoinositide 3-kinase (PI3K)–protein kinase B (Akt) pathway [*2*–*10*]. Both pathways are initiated by Src family kinases (SFKs), with c-Src, Fyn, and Yes among the most widely expressed [*11*–*13*]. Pharmacological inhibition of SFKs abolished BPC-157–induced angiogenesis in vitro, underscoring their mechanistic relevance [*5*]. Likewise, ERK inhibition blocked BPC-157–driven migration, proliferation, and tube formation in endothelial cells [*8*]. In addition, Dynasore, an inhibitor of dynamin-dependent endocytosis, prevented BPC-157–induced angiogenesis by impairing vascular endothelial growth factor receptor 2 (VEGFR2) internalization and downstream signaling [*4*].

In vitro, BPC-157 is active at nanomolar to micromolar concentrations, initiating SFK–FAK–ERK and Src–PI3K–Akt signaling across multiple cell types. In tendon fibroblasts, 100 nM–1 μM enhanced migration and stress resistance, with maximal FAK/paxillin phosphorylation observed at 1 μM [*6*]. In endothelial cells, 500 nM–1 μM promoted Src-dependent endothelial nitric oxide synthase (eNOS) phosphorylation and nitric oxide (NO) production [*5*]. In myoblasts, 70 nM–1.4 μM increased spreading and paxillin phosphorylation [*10*]. In fibroblasts, co-treatment with growth hormone (GH) upregulated GH receptor expression and proliferative signaling beginning at 100 nM [*7*].

Collectively, in vitro studies demonstrate that BPC-157 promotes migration, collagen deposition, angiogenesis, and survival under stress through ERK and Akt signaling

(*Supplementary Table S1*) [*2–10*]. In vivo, these mechanisms translate into accelerated repair of tendon, muscle, skin, gastrointestinal mucosa, brain, and spinal cord, with consistent hallmarks including nitric oxide synthase (NOS) activation, enhanced angiogenesis, resolution of inflammation, and rapid wound closure (*Supplementary Table S2*) [*2–3,14–19*].

Notably, ERK signaling in response to BPC-157 treatment appears to be context-dependent. While ERK activity supports tissue repair, excessive or unregulated ERK signaling is a well-established oncogenic driver [*20*]. Skiret et al. [*21*] reported that BPC-157 suppressed ERK phosphorylation and inhibited tumor growth in melanoma cells, in contrast to its stimulatory effects on ERK and proliferation in regenerative models. How BPC-157 differentially modulates ERK activity, activating in regenerative contexts while suppressing ERK signaling in a melanoma model, remains to be determined.

At the transcriptional level, BPC-157 orchestrates coordinated gene expression programs downstream of SFK–FAK–ERK and Src–PI3K–Akt signaling. In rat skin wounds, BPC-157 upregulated repair-associated genes including *Akt1* (Akt), *Braf*, *Egfr*, *Egr1*, *Grb2*, *Hdac7*, *Kras*, *Mapk1/3* (ERK-2/1), *Mapk14*, *Nos3*, *Pik3cd* (PI3K), *Ptk2* (FAK), *Pxn* (paxillin), *Src*, *Srf*, and *Vegfa* [*9*]. In hippocampal ischemia, BPC-157 increased *Akt1*, *Egr1*, *Foxo*, *Nos1/3*, *Src*, *Srf*, and *Vegfr2* while suppressing *Nos2* and *Nfkb1*, correlating with improved neurological outcomes [*16*]. In spinal cord injury, BPC-157 rapidly induced *Nos1/2/3* and *Ptgs2* (COX-2), reducing edema and hematoma [*17*]. Collectively, these transcriptional profiles implicate both the VEGF–Akt–hypoxia-inducible factor 1α (HIF-1α) pathway and FAK–ERK signaling. HIF-1α promotes pro-angiogenic transcriptional programs (*Vegfa*, *Ptgs2*, *Nos* isoforms) [*25–27*], while activated ERK drives immediate-early gene expression (*Fos*, *Jun*, *Egr1*, *Srf*) [*27*]. Thus, the FAK–ERK and PI3K–Akt axes connect extracellular cues to pro-repair gene expression programs, supporting cell survival, proliferation, migration, and angiogenesis — mechanistic effects consistent with those observed following BPC-157 treatment [*9,16,17,22–27*].

Despite these mechanistic insights, the receptor(s) and direct binding partners of BPC-157 remain unidentified. To address this gap, a structural model was developed to guide screening for receptor domains associated with its known cellular effectors. In parallel, a novel fluorescent fusion protein, mCherry–BPC157$_2$, was engineered and validated, providing a versatile tool for future functional assays aimed at mapping the BPC-157 interactome.

1.2
Src Family Kinase Structure, Expression Patterns and Functional Roles

SFKs are non-receptor tyrosine kinases that integrate extracellular and intracellular signals to promote proliferation, migration, angiogenesis, and tissue repair through two converging cascades: FAK–ERK and PI3K–Akt [*11–13,22–24*]. ERK activation drives keratinocyte migration and fibroblast activation, with fibroblasts remodeling the extracellular matrix via increased matrix metalloproteinase activity and collagen secretion, thereby initiating wound healing [*23,24*]. In peripheral nerves and related tissues, ERK signaling further supports axon outgrowth, anti-apoptotic survival, and epigenetic reprogramming during regeneration [*28*]. Importantly, c-Src overexpression accelerates wound closure via ERK-dependent mechanisms, whereas inhibition of either c-Src or ERK impairs tissue healing and cell proliferation [*29,30*].

In parallel, SFKs, predominantly c-Src, initiate the Src–PI3K–Akt cascade, a critical pathway governing cytoprotection and tissue regeneration [*23,24,31–33*]. Upon activation, c-Src phosphorylates scaffold and adaptor proteins, enabling PI3K recruitment and activation at the plasma membrane. PI3K then catalyzes the conversion of phosphatidylinositol 4,5-bisphosphate (PIP2) into phosphatidylinositol 3,4,5-trisphosphate (PIP3), a lipid second messenger that recruits Akt to the membrane [*34–38*]. Akt is subsequently phosphorylated by upstream kinases, including c-Src, and in turn phosphorylates diverse downstream effectors that collectively enhance cell survival, proliferation, and angiogenesis [*34–38*]. A pivotal Akt substrate is eNOS, whose phosphorylation stimulates nitric oxide NO production, promoting vasodilation, increased blood flow, and improved oxygen and nutrient delivery to regenerating tissues [*25,36–39*].

c-Src is broadly expressed in epithelial cells, fibroblasts, and endothelial cells, where it coordinates adhesion dynamics, motility, and growth factor responses; its dysregulation is tightly linked to tumor progression [*11–13,40*]. Fyn, while also widely distributed, is strongly enriched in the central nervous system (CNS), where it governs neuronal differentiation, synaptic plasticity, and myelination. Beyond the CNS, Fyn contributes to integrin-dependent signaling in fibroblasts and mast cells, driving cytoskeletal remodeling and motility [*13,41*]. Yes, similarly ubiquitous, exerts specialized vascular functions by modulating endothelial junctional stability and barrier integrity through VE-cadherin phosphorylation and endocytosis, thereby shaping vascular remodeling [*13,42*]. In contrast, lineage-restricted SFK members such as Hck are confined to hematopoietic cells, including monocytes, macrophages, and neutrophils, where Hck mediates proliferation and immune-specific signaling [*11,43*].

SFKs exhibit a conserved modular architecture consisting of an N-terminal SH4 domain, an intrinsically disordered region, tandem SH3 and SH2 domains, and a C-terminal kinase domain [*11–13,44,45*]. This arrangement supports regulation through both intramolecular and membrane-associated interactions. For instance, caveolin-1 (Cav-1) sequesters SFKs at the plasma membrane in their inactive state, positioning them adjacent to Cav-1–bound eNOS [*46,47*]. This arrangement enables rapid NO production once activated SFKs phosphorylate eNOS directly [*48-50*].

Activation by SH2 or SH3 domain ligands enables SFKs to phosphorylate FAK, forming SFK–FAK complexes at integrin-rich adhesion sites [*22*]. FAK autophosphorylation generates a high-affinity docking site for the SFK SH2 domain, reinforcing kinase recruitment and promoting adaptor protein phosphorylation, which initiates the ERK signaling cascade [*23,24*]. SFK activation can precede FAK phosphorylation as seen in growth factor receptor–driven contexts, whereas in adhesion-driven signaling, phosphorylated FAK often recruits and activates SFKs, highlighting bidirectional regulation [*11,22,24*].

Beyond receptor-coupled signaling, SFKs also mediate ligand-independent receptor transactivation. For example, SFKs phosphorylate epidermal growth factor receptor and human epidermal growth factor receptor 2 cytoplasmic tails during extracellular matrix rigidity sensing, a mechanotransduction pathway driven by SH3 domain–mediated SFK activation [*51,59*]. This event promotes cell spreading, migration, and proliferation independent of external growth factors. Similarly, VEGFR2 can undergo ligand-independent transactivation through SFK-dependent phosphorylation [*32,52*].

In summary, SFKs serve as central regulators of cellular stress responses, integrin activation, and growth factor signaling, shaping outcomes following tissue injury and stimulation. Positive cross-talk between the SFK–FAK–ERK and Src–PI3K–Akt pathways act synergistically to promote tissue protection, repair, and remodeling—mechanisms that parallel those observed with BPC-157 treatment [*2–10,14–19,23–25,28–30,37*].

1.3
Src Family Kinase Autoinhibition, Regulation and SH3 Domain-Mediated Activation by Proline-Rich Ligand

SFKs maintain autoinhibition through two intramolecular clamps: the SH2 domain binds a phosphorylated tyrosine on the C-terminal tail, while the SH3 domain engages a polyproline II (PPII) helix formed within the SH2–kinase linker region, together constraining kinase activity [*13,53–56*]. Activation occurs when proline-rich ligands—such as β-arrestin1, integrin β3 cytoplasmic tails, p130Cas, or viral proteins like HIV-1 Nef—bind the SH3 domain, displace the intramolecular clamp, and induce an open, catalytically active kinase conformation [*57–64*]. In FAK signaling, SFK SH3 domain binding to the p130Cas PPII motif both anchors and activates SFKs, enabling rapid multisite phosphorylation of p130Cas and other adaptor proteins, thereby reinforcing FAK signaling [*58,62*]. Notably, p130Cas contains both PPII helix motifs and SH3 domains, positioning it as a significant central adapter in FAK-related pathways.

In the context of SH3 domain ligands, PR-39—a 39-residue proline-rich peptide originally isolated from porcine intestine—provides a compelling precedent. A 15-amino acid N-terminal fragment, PR-39(15) (*RRRPRPPYLPRPRPP*), was shown to associate with the plasma membrane, penetrate endothelial cells, and selectively bind intracellular SH3 domain-containing proteins [*65*]. Detailed characterization revealed that PR-39(15) engaged the SH3 domain of p130Cas and altered its subcellular distribution in a state consistent with activation of p130Cas-dependent pathways [*65*]. This example underscores how short proline-rich ligands can be internalized and subsequently engage SH3 domains, thereby activating downstream intracellular signaling cascades.

Activation of SFKs via their SH2 domains occurs when the intramolecular inhibitory interaction between the SH2 domain and the phosphorylated C-terminal tail is displaced by an external phosphotyrosine-containing ligand. Such ligands are commonly presented by activated receptor cytoplasmic tails or integrins [*11–13,24*]. Importantly, the binding of a ligand to either the SH2 or SH3 domain can partially or fully relieve autoinhibition, thereby inducing SFK autophosphorylation at Tyr419 (in human c-Src) [*53-55*]. This autophosphorylation event further stabilizes the active SFK conformation, supporting downstream signaling [*53*].

In addition to the intramolecular clamps, SFK activity is tightly regulated by C-terminal Src kinase (Csk), a cytoplasmic tyrosine kinase that phosphorylates a conserved tyrosine residue on the SFK C-terminal tail (Tyr530 in human c-Src) [*66*]. This phosphorylation event

initiates the SH2–tail binding reaction, reinforcing the inactive, closed conformation. Csk activity is initiated by recruitment to the plasma membrane via adaptor proteins, providing spatial and temporal control of SFK inhibition [*66*]. One intriguing possibility is that BPC-157 could interfere with Csk localization by competing for the Csk SH3 domain, thereby disrupting adaptor protein interactions and reducing Csk-mediated phosphorylation of SFKs. However, direct cellular evidence of SH3-mediated Csk inhibition is lacking, and in silico modeling suggests a weaker association of BPC-157 with the Csk SH3 domain (data not shown).

In summary, SH3 domain ligands are capable of relieving SFK autoinhibition, with SH2 and SH3 domain ligands often acting cooperatively to potentiate SFK localization and activation [55,*56*]. Within this mechanistic framework, BPC-157 may act as a proline-rich SH3 domain ligand, competitively disrupting the autoinhibitory SH3–linker interaction to enhance membrane targeting and trigger downstream signaling (*Figure 1)*. Activated SFKs then initiate parallel healing cascades, including FAK–ERK and PI3K–Akt pathways, while also prompting NO production from eNOS via SFK phosphorylation of the Cav-1–eNOS complex (*Figure 2*).

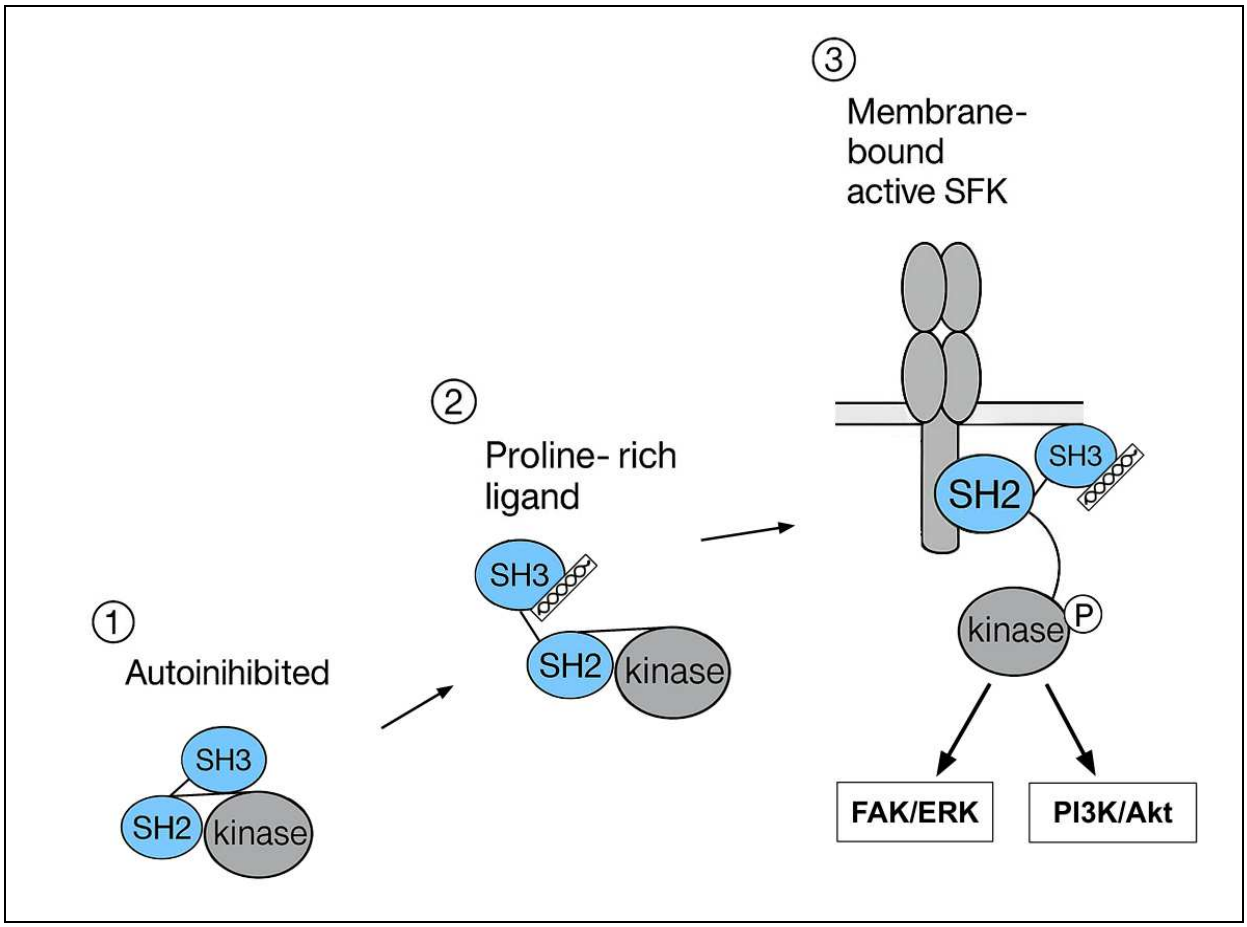

Figure 1. Mechanism of Src family kinase activation by proline-rich ligand. (1) Autoinhibition: In the inactive state, the SH3 domain binds the SH2–kinase linker, and the SH2 domain binds a C-terminal tail phosphotyrosine residue, keeping Src family kinases (SFKs) autoinhibited. (2) Ligand Binding: A proline-rich ligand binds to the SH3 domain, disrupting the autoinhibited conformation and allowing for SH2 domain interaction with phosphotyrosines on partially activated receptors. (3) Membrane Activation: Binding of the SH2 domain facilitates recruitment of SFKs to the membrane. Upon SH2 domain binding, autophosphorylation within the activation loop fully activates SFKs, initiating downstream signaling cascades via the focal adhesion kinase (FAK)–extracellular signal-regulated kinase (ERK) and the phosphoinositide 3-kinase (PI3K)–protein kinase B (Akt) pathways. Abbreviations: Akt, protein kinase B; ERK, extracellular signal-regulated kinase; FAK, focal adhesion kinase; PI3K, phosphoinositide 3-kinase; SFK, Src family kinase; SH2/SH3, Src homology 2/3 domains.

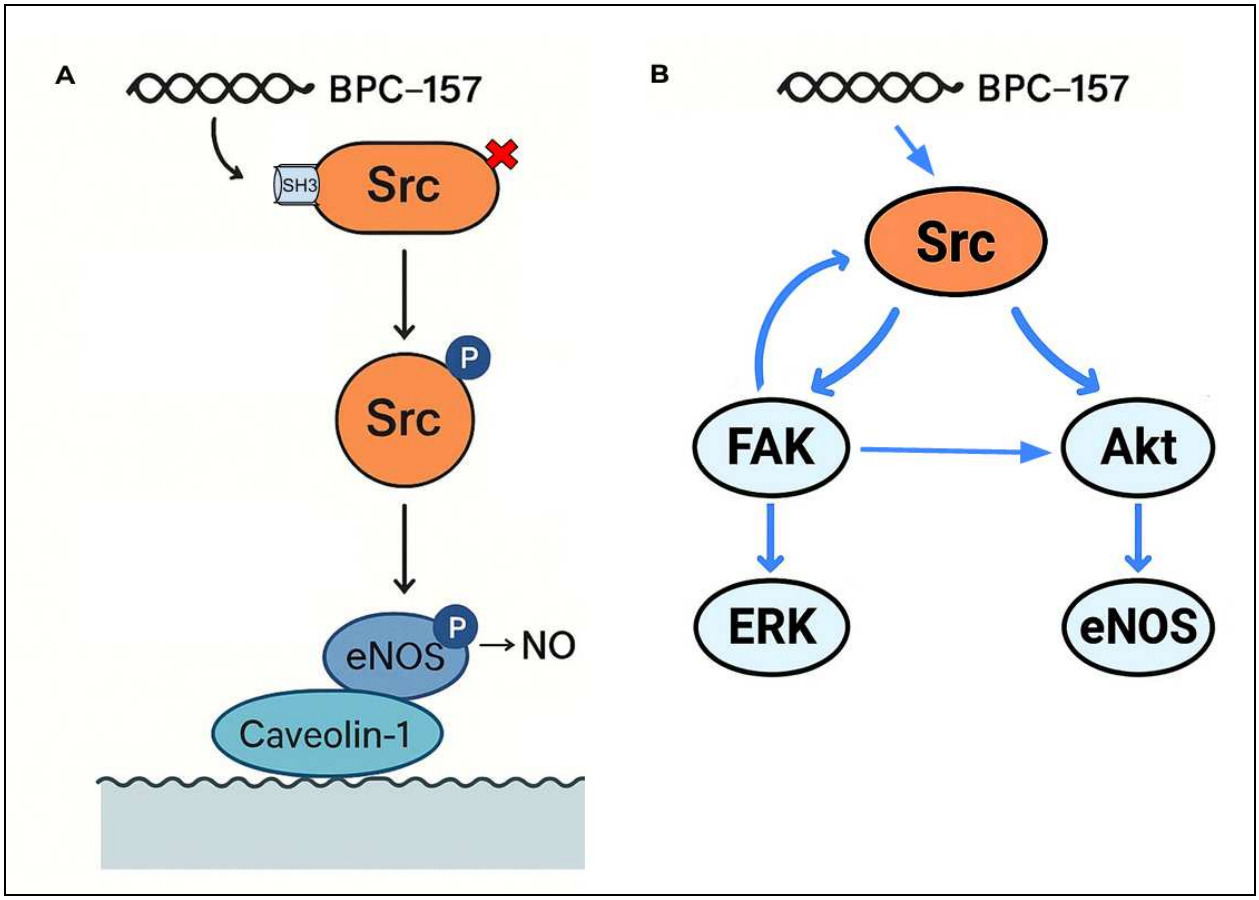

Figure 2. Proposed mechanism of BPC-157–induced Src activation and parallel healing pathways. (A) BPC-157 is proposed to bind the SH3 domain of Src (Src family kinases; c-Src, Fyn, and Yes), disrupting the autoinhibitory conformation and facilitating autophosphorylation of the catalytic domain. Phosphorylated Src subsequently displaces the inhibitory caveolin-1–endothelial nitric oxide synthase (eNOS) complex via direct phosphorylation of eNOS, leading to nitric oxide (NO) production. This model is based on the findings reported by Hsieh et al. [*5*]. (B) Src activation by BPC-157 triggers focal adhesion kinase (FAK) and protein kinase B (Akt) signaling pathways. FAK activation reinforces Src signaling via a positive feedback loop and promotes extracellular signal-regulated kinase (ERK) activation. Activated FAK can also initiate Akt signaling. Involvement of phosphoinositide 3-kinase is not shown. Arrows indicate activation. Abbreviations: Akt, protein kinase B; ERK, extracellular signal-regulated kinase; eNOS, endothelial nitric oxide synthase; FAK, focal adhesion kinase; NO, nitric oxide; SH3, Src homology 3 domain; Src, Src family kinase (c-Src, Fyn, and Yes).

1.4
Affinity Ranges for SH3 Domain–Mediated Src Family Kinase Autoinhibition

Binding of SH3 domains to proline-rich PPII ligands typically occurs with moderate affinity, displaying dissociation constants (K_D) in the low- to mid-micromolar range (~3–20 μM) [*55,56,67,68*]. In SFKs, however, autoinhibition is preserved through a higher-affinity intramolecular interaction between the SH3 domain and the PPII helix within the SH2–kinase linker region. Biophysical measurements and structural modeling indicate that this SH3–linker interaction exhibits K_D values in the nanomolar to low-micromolar range (~0.3–1 μM) [*69*–*71*]. Having a naturally stronger autoinhibitory interaction is essential for stabilizing the closed, inactive state of SFKs, thereby preventing premature kinase activation and aberrant proliferative signaling.

Several viral and cellular ligands can outcompete this autoinhibitory interaction through high-affinity SH3 domain binding. As mentioned in Section 1.3, the HIV-1 accessory protein Nef binds the Hck SH3 domain with submicromolar affinity (K_D ~0.14–0.44 μM) [*69*]. This binding event displaces the intramolecular SH3–linker clamp and promotes kinase activation without requiring SH2-tail release [*60*]. Nef also activates other SFKs through SH3 displacement, such as c-Src, albeit with lower affinity (K_D ~5 μM) [*63,64*]. Similarly, integrin β3 cytoplasmic tails, p130Cas PPII motifs, and synthetic peptides have been shown to engage SFK SH3 domains with affinities in the low-micromolar range, sufficient to trigger FAK signaling and downstream ERK activation [*55,58,61,67*]. For example, the synthetic peptide VSL12 (*VSLARRPLPPLP*) binds c-Src, Fyn, Hck, and Lyn SH3 domains with low-micromolar to submicromolar affinity, displaces the native SH3–linker clamp, and fully activates all four SFKs in vitro [*55*]. Notably, even autophosphorylated c-Src and Hck remained susceptible to further activation by SH3 domain displacement, underscoring SH3 domain engagement as an independent and potent regulatory axis for some SFK members [*55,56*].

Collectively, these findings demonstrate that SH3 domain ligands at sub-micromolar concentrations can override intramolecular SFK autoinhibition, establishing a precedent for proline-rich peptides to function as SH3 domain agonists and initiate SFK-dependent signaling cascades.

1.5
Molecular and Structural Basis of SH3 Domain Interactions

SH3 domains are compact protein modules of ~60 amino acids, commonly present in adaptor proteins and signaling molecules [*70*]. They recognize proline-rich ligands that traditionally adopt a PPII helix motif. Two canonical ligand classes are defined: Class I (*R/K–x–x–P–x–x–P*) and Class II (*P–x–x–P–x–R/K*), where "*x*" denotes any amino acid. These motifs bind the SH3 groove in opposite orientations, thereby contributing to both affinity and specificity [*70*–*74*].

BPC-157 contains a lysine residue within its core PPII motif (*PPPGKP*). This feature, together with the peptide's compact size, may permit recognition by SH3 domains that accommodate either Class I or Class II ligands. Such dual-class compatibility aligns with proteome-wide screening data indicating that nearly half of SH3 domains can engage noncanonical sequences [*73*]. Among Src family kinases, c-Src exemplifies this versatility, binding ligands from both classes [*75*].

Structurally, SH3 domains adopt a conserved β-sandwich fold composed of five or six β-strands arranged into two orthogonal, antiparallel β-sheets. This architecture stabilizes a hydrophobic core and generates a ligand-binding surface defined by three flexible loops: RT, n-Src, and distal [*72*]. Together, these loops form a groove that accommodates PPII helices through interactions with aromatic SH3 domain residues such as tryptophan and tyrosine. Binding specificity is further refined by charged residues flanking the ligand's *PxxP* motif, which engage the RT, n-Src, and distal loops to fine-tune recognition [*70*–*75*].

Consistent with this structural framework, Hou et al. [*81*] computationally demonstrated that van der Waals (vdW) contacts provide the dominant energetic contribution to ligand affinity within the Abl kinase SH3 domain. Specifically, hydrophobic residues located in the RT loop, groove floor, and distal loop (analogous to Tyr0, Trp28, and Tyr46 SH3 domain residues) form a tightly packed, non-bonded contact interface against the ligand's PPII helix. In contrast, hydrogen bonding and electrostatic forces were found to primarily orient the ligand rather than drive binding affinity [*81*].

1.6
Comparative Analysis of SH3 and Other Proline-Rich Ligand Binding Domains

The proposed affinity of BPC-157 for SH3 domains is consistent with the permissive binding characteristics and broader sequence tolerance of this receptor module. In contrast, other PPII-recognition domains, such as WW and Ena/VASP Homology 1 (EVH1), display more stringent sequence requirements [*76,77*]. WW domains preferentially recognize proline- and aromatic-rich motifs centered on *PPxY* consensus sequences, which are distinct from canonical SH3-binding motifs [*76*]. EVH1 domains exhibit even greater specificity, binding FP4 motifs (*FPPPP*) [*77*].

Collectively, structural and biochemical analyses indicate that the N-terminal PPII segment of BPC-157 lacks the consensus motifs required for high-affinity binding to WW or EVH1 domains, thereby reinforcing SH3 domains as the most plausible interaction partners.

2.0
Results

2.1
BPC-157 Structural Model

The N-terminal segment of BPC-157 (*GEPPPGKP*) is notably proline-rich, containing 50% proline residues, a composition that favors adoption of a PPII helical conformation. In silico modeling supported this structural tendency (*Figure 3*), predicting a left-handed helix conformation with approximately three residues per turn and characteristic backbone dihedral angles ($\varphi \approx -75°$, $\psi \approx 150°$) [*74*]. The predicted structural ensembles of the peptide displayed minimal conformational variability, particularly within the proline-rich region (*Supplementary Image S1*), indicating a stable and conserved PPII structure.

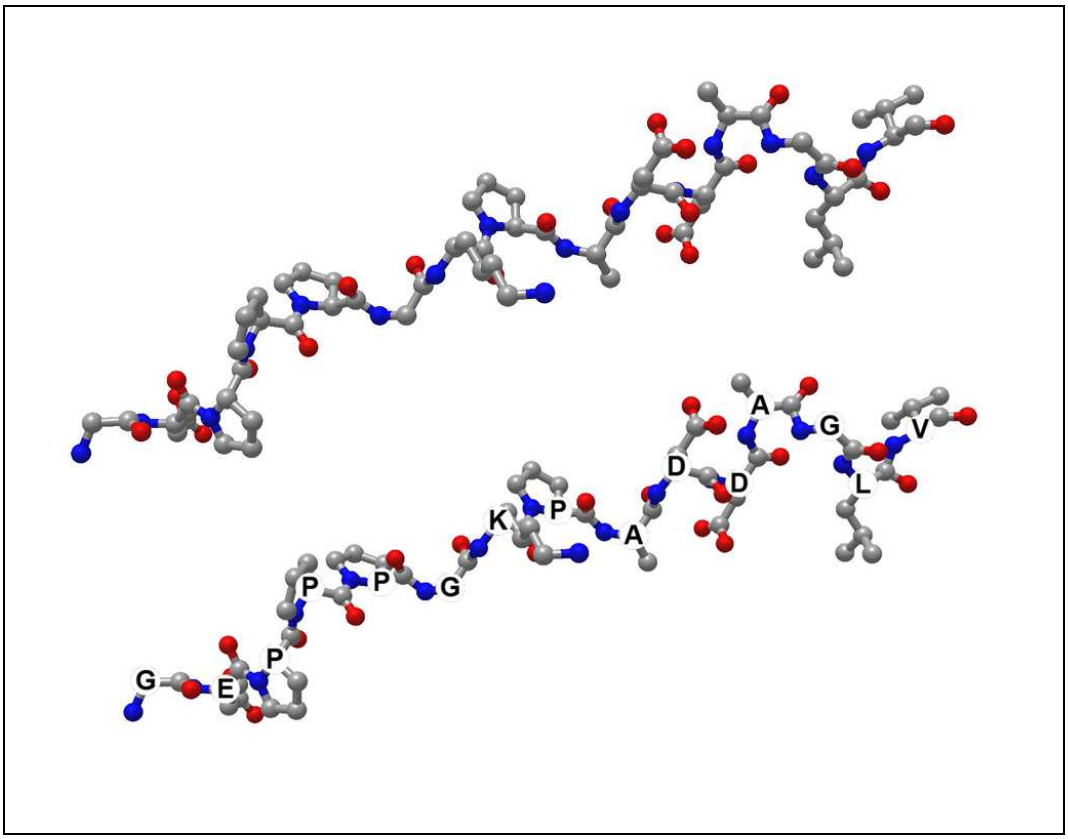

Figure 3. Predicted three-dimensional structure of BPC-157. (Top panel) Predicted BPC-157 tertiary structure indicating a polyproline II helix conformation. (Bottom panel) Structure annotated with the BPC-157 amino acid sequence *GEPPPGKPADDAGLV*. Atom colors are carbon (grey), oxygen (red), and nitrogen (blue).

2.2
SH3 Domain Binding Models

In silico docking revealed biologically plausible binding conformations wherein BPC-157's PPII helix was accommodated within the SH3 domain binding groove (*Figure 4*). To initially validate the binding prediction workflow, a 15-residue peptide segment from the SH2–linker region of full-length c-Src was similarly modeled and docked to the c-Src SH3 domain. Comparative analysis revealed this method accurately recapitulated the established binding orientation and key residue contacts observed in full-length, autoinhibited c-Src [*54*,*55*,*75*,*78*–*80*], lending support to the predicted BPC-157 binding models.

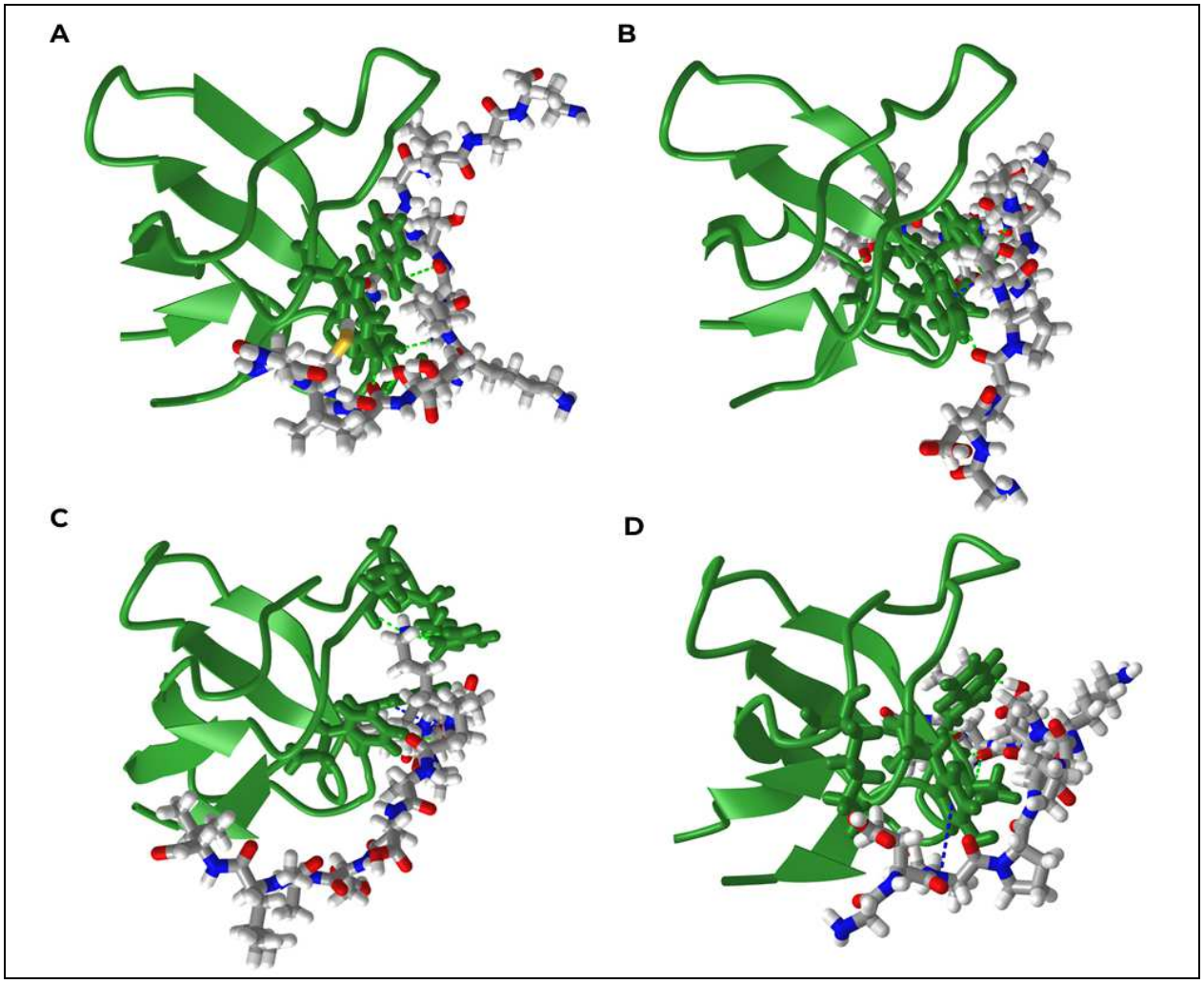

Figure 4. In silico docking of BPC-157 and c-Src SH2-linker peptide within SFK SH3 domain binding grooves. (A) Predicted autoinhibited conformation of c-Src SH3 domain bound to SH2-linker peptide. (B) Predicted BPC-157 binding to c-Src SH3 domain, oriented N- to C-terminus. (C) Predicted BPC-157 binding to Yes SH3 domain, oriented C- to N-terminus. (D) Predicted BPC-157 binding to Fyn SH3 domain, oriented N- to C-terminus. SH3 domains are shown as green ribbons, peptides in atom colors (carbon, grey; oxygen, red; nitrogen, blue; sulfur, yellow). Interacting SH3 residues are depicted as sticks. Dotted lines indicate predicted interactions: red, cation–π; blue, π–π stacking; green, hydrogen bonds. PDB identifiers of SH3 domains analyzed: c-Src (1SRL), Yes (2HDA), Fyn (1NYF). Abbreviation: SH3, Src homology 3 domain.

2.3
Interaction Analysis

Docking orientation and interaction analysis revealed that the modeled SH2-linker sequence engages the c-Src SH3 domain in a manner that recapitulates residue-contact patterns observed in autoinhibited c-Src. Conserved SH3 domain analogues, including Tyr0, Tyr2, Asp9, Asp27, Trp28, and Pro43, were involved in the predicted binding interface [*54,55,57,74,75,78-80*].

Binding models of BPC-157 with SFK SH3 domains demonstrated conserved contacts within the canonical SH3 binding groove as well, notably Tyr0, Tyr2, Trp28, and Tyr46 analogues. Stabilizing polar interactions were observed with residues in the RT loop (Asp1, Glu3, Arg5, Thr6, Asp9, Lys14) and the n-Src loop (Asn23, Glu25, Asp27), while Pro43 and Asn45 in the distal loop contributed to the binding interface in select models. Collectively, the RT, n-Src, and distal loops, together with the Trp28 analogue on the groove floor, have been previously identified as key determinants of ligand specificity and affinity for SFK SH3 domains [*54,55,57,70-75,78-81*]. Accordingly, the predictive binding models presented indicate that both SH2-linker–c-Src SH3 domain and BPC-157–SFK SH3 domain interactions conform to canonical SH3 domain binding modes (*Table 1*).

Table 1. Comparative predicted contacts of BPC-157 and Src SH2-linker peptide to SFK SH3 domains. Conserved SH3 domain residues are listed under "Residue #," with numbering referencing groove-entry tyrosine (Tyr0). Each row denotes the analogous amino acid by residue number from corresponding SH3 domain Protein Data Bank files. Amino acids listed are predicted to exhibit non-bonded contacts with the peptide ligand. Total interaction contacts (TIC) represent the sum of all non-bonded contacts. Interaction score (IS) was calculated using a heuristic weighting scheme: non-bonded contacts were counted, with additional weights assigned for π–π stacking (+3), cation–π (+4), and hydrogen bonds (+5), reflecting relative energetic contributions reported in literature [*84–86*]. Additional interaction types are abbreviated as: π-S, π–π stacking; π-C, cation–π; HB, hydrogen bond. An asterisk (*) indicates multiple interactions at that residue.

SH3 Domain Residue #	**SH2 Linker-cSrc (Fig 5-A)**	**BPC157-cSrc (Fig 5-B)**	**BPC157-Yes (Fig5-C)**	**BPC157-Fyn (Fig5-D)**	**Structural Location**
Tyr0	Tyr14^{HB}	Tyr14	Tyr100	Tyr91$^{π\text{-}S}$	RT loop
Asp1		Asp15	Asp101		RT loop
Tyr2	Tyr16	Tyr16	Tyr102	Tyr93	RT loop
Glu3		Glu17	Glu103^{HB}		RT loop
Arg5		Arg19	Arg105 ^{HB*2}	Arg96	RT loop
Thr6	Thr20	Thr20			RT loop
Asp9	Asp23	Asp23		Asp100	RT loop
Lys14	Lys28			Lys105$^{π\text{-}C}$	RT loop
Asn23	Asn37	Asn37^{HB}			n-Src Loop
Glu25		Glu39	Glu125		n-Src Loop
Asp27	Asp41^{HB*2}	Asp41^{HB}	Asp127	Asp118^{HB}	n-Src Loop
Trp28	Trp42^{HB}	Trp42^{HB}	Trp128$^{π\text{-}S*2}$	Trp119^{HB*2}	Groove floor
Pro43	Pro57		Pro143	Pro134	Distal loop
Asn45	Asn59^{HB}		Asn145		Distal loop
Tyr46		Tyr60$^{HB,π\text{-}S}$	Tyr146^{HB*2}	Tyr137	Distal loop
TIC	107	118	129	90	
IS	132	141	160	112	

2.4
Interaction Analysis Summary

Interaction analysis across SH3 domain regions, including the RT loop (Tyr0–Lys14), n-Src loop (Asn23–Asp27), groove floor (Trp28), and distal loop (Pro43–Tyr46), revealed consistent patterns of peptide engagement across all models. To quantify these interactions, an interaction score (IS) was derived using a heuristic weighting scheme: non-bonded contacts were enumerated, with additional weights assigned for π–π stacking (+3), cation–π interactions (+4), and hydrogen bonds (+5), reflecting their relative energetic contributions [*84-86*]. While not expressed in kcal/mol, these scores provide a comparative framework for identifying potentially relevant interactions.

Predicted binding of the SH2-linker to the c-Src SH3 domain showed strong engagement across all key SH3 domain regions, forming hydrogen bonds with Tyr0, Trp28, Asn45, and a double hydrogen bond with Asp27. Additional non-bonded contacts with the Tyr2, Thr6, Asp9, Lys14, Asn37, and Pro57 analogues align with the known autoinhibited conformation of c-Src [*54*,*55,75,78–80*].

Similarly, docking predictions for BPC-157 to the c-Src SH3 domain revealed extensive interactions, particularly within the RT loop (Tyr0, Asp1, Tyr2, Glu3, Arg5, Thr6, Asp9), as well as hydrogen bonds with Asn23, Asp27, Trp28, and Tyr46. Both BPC-157 and the SH2-linker model shared hydrogen bonding with the Asp27 and Trp28 analogues, underscoring conserved engagement at the groove floor and n-Src loop. Despite forming one fewer hydrogen bond overall, BPC-157 achieved a higher interaction score, driven by its broader engagement across RT loop residues.

In the BPC-157–Yes SH3 model, BPC-157 adopted a reversed C- to N-terminal orientation relative to c-Src, yet maintained extensive RT loop engagement, including a double hydrogen bond with Arg5. This complex contacted 60% of SH2-linker–c-Src residues and 75% of BPC-157–c-Src residues. Double π–π stacking with Trp28 and hydrogen bonds with Glu3, Arg5, and Tyr46 analogues contributed to the highest interaction score observed (160).

BPC-157 predicted interaction with the Fyn SH3 domain involved fewer contacts but retained engagement with key functional regions. In the N- to C-terminal orientation, the model formed a π–π stacking interaction with Tyr0, a cation–π interaction with Lys14, and hydrogen bonds with Asp27 and Trp28. Additional non-bonded contacts included Tyr2, Arg5, Asp9, Pro43,

and Tyr46. Though the interaction score was lower (112), the distributed nature of contacts supports a plausible binding mode.

In summary, modeled interactions between BPC-157 and SFK SH3 domains, as well as SH2-linker binding to the c-Src SH3 domain, consistently engaged essential ligand recognition residue analogues—Tyr0 and Tyr2 in the RT loop, Asp27 in the n-Src loop, and Trp28 at the groove floor—supporting a shared recognition motif. Collectively, these comparative insights support BPC-157's potential to engage SH3 domains via biologically relevant binding modes.

2.5 mCherry–BPC157$_2$ Validation

Validation of the mCherry–BPC157$_2$ fusion construct was assessed by fluorescent imaging and immunoblotting. *Spodoptera frugiperda* (Sf9) cells displayed robust, time-dependent mCherry fluorescence over 7 days post-baculovirus infection, confirming successful expression of a fluorescent fusion protein.

Immunoblot analysis of lysates harvested 5 days post-infection revealed bands migrating below the 39 kDa marker, consistent with the predicted molecular weights of mCherry–BPC157$_2$ (30.7 kDa processed; 33.1 kDa unprocessed with N-terminal melittin sequence). The strongest signal was observed between ~31–34 kDa, accompanied by less concentrated bands corresponding to truncated species at ~29 kDa (single-tail mCherry–BPC-157) and ~26.6 kDa (mCherry domain). A weaker band at ~85 kDa was also detected, likely reflecting oligomerization (*Supplementary File S27*). Collectively, these findings demonstrate robust expression of full-length mCherry–BPC157$_2$, accompanied by processing intermediates and truncated products (*Figure 5*).

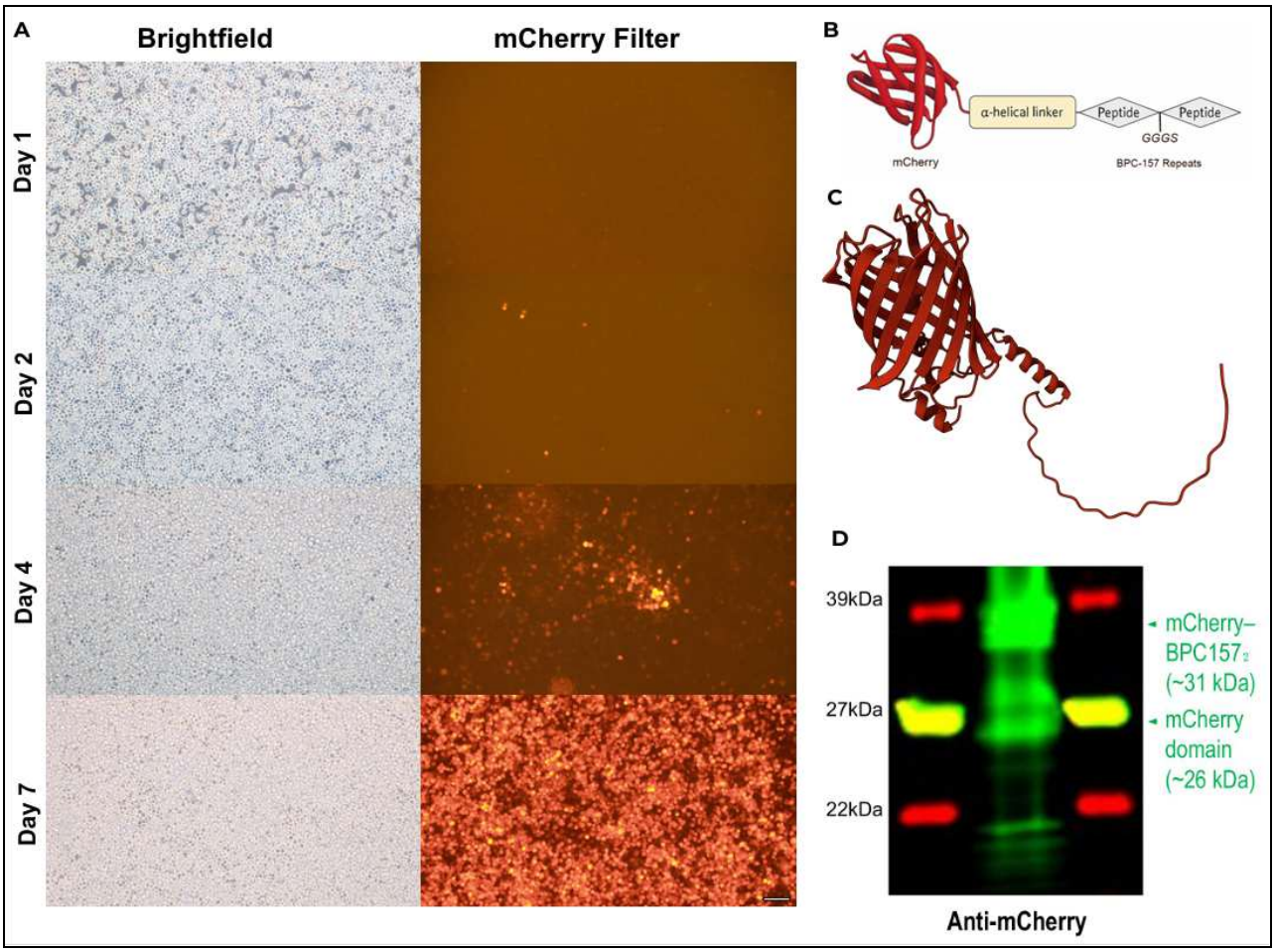

Figure 5. Validation of mCherry–BPC157$_2$ expression in Sf9 cells: fluorescence imaging, structural prediction, and immunoblot analysis. (A) Time course of mCherry fluorescence in Sf9 cells following baculovirus transduction. Brightfield and corresponding fluorescence images (530–550 nm Hg lamp excitation) were captured at days 1, 2, 4, and 7 post-infection. Scale bar = 100 µm, consistent across all panels. (B) Schematic representation of the mCherry–BPC157$_2$ fusion protein. (C) Predicted 3D structure of mCherry–BPC157$_2$ generated with AlphaFold3. (D) Immunoblot of transduced Sf9 cell lysates probed with a polyclonal anti-mCherry antibody. Lane 2 shows a band cluster at ~31–34 kDa, consistent with the predicted full-length fusion (30.7 kDa). Higher-migrating species correspond to ER-processing variants retaining the N-terminal secretory sequence (33.1 kDa) and putative post-translationally modified forms. Additional bands at ~29 kDa (single-tail mCherry–BPC157) and ~26.6 kDa (mCherry domain) indicate truncated fragments. Prestained molecular weight markers (22, 27, 39 kDa) are shown in Lanes 1 and 3. Abbreviation: Sf9, *Spodoptera frugiperda* cells.

3.0
Discussion

Despite extensive preclinical studies supporting its regenerative capacity, the precise molecular mechanisms underlying BPC-157's pleiotropic pro-repair effects remain undefined. A central unresolved question is whether BPC-157 acts through an extracellular receptor, via direct intracellular interactions, or through a combination of both. The robust regenerative and cytoprotective phenotypes observed across diverse cell types and tissues suggest the existence of a conserved molecular interaction linking BPC-157 to canonical ERK and Akt signaling cascades.

Here, an integrative approach combining computational modeling, in silico docking, and interaction analysis supports a model in which the proposed PPII helix motif of BPC-157 engages the SH3 domains of SFKs, notably c-Src, Yes, and Fyn. Occupation of the SH3 domain interaction surface by BPC-157 destabilizes the autoinhibitory SH3–linker clamp, increases SH2 domain sampling, and thereby primes SFKs for activation. Upon SH2 domain engagement with phosphotyrosine motifs, primed SFKs undergo activation-loop autophosphorylation and initiate FAK–ERK and PI3K–Akt signaling. Notably, in some cellular contexts, SH3 domain engagement alone is sufficient to fully activate SFKs [*55-62*].

Once activated, SFKs disrupt the inhibitory Cav-1–eNOS complex by phosphorylating eNOS, resulting in NO production [*46-49*]. Simultaneously, activated SFKs initiate the FAK–ERK and PI3K–Akt signaling pathways to promote cell survival, proliferation, migration, and tissue repair [*11,12,23,24,30-33*]. Activated Akt similarly phosphorylates eNOS, which results in additional NO production [*35*], and SFK-driven ERK/Akt-mediated gene transcription programs further support tissue regeneration [*25-27*]. Taken together, direct SFK activation by BPC-157 provides a coherent explanation for the broad cytoprotective, angiogenic, and reparative effects observed across preclinical models (*Supplementary Tables S1, S2*) [*2-10,14-19*].

A strong precedent for this mechanism is provided by the HIV-1 accessory protein Nef, which activates SFKs by engaging SH3 domains through a PPII helix motif [*63,64*]. Similarly, integrin β3 cytoplasmic tails activate c-Src via SH3 domain binding [*61*]. Most relevant to the present hypothesis, PR-39—a 39-amino acid proline-rich peptide originally isolated from digestive tissues and structurally reminiscent of BPC-157—has demonstrated intracellular SH3 domain binding and angiogenesis effects in vivo [*65*,*82*]. As discussed in Section 1.3, a

15-amino acid N-terminal fragment of PR-39 was shown to interact with the plasma membrane, enter endothelial cells via non-specific endocytosis, and bind to intracellular SH3 domain-containing proteins [*65*]. Notably, Li et al. [*82*] demonstrated that PR-39 stabilizes HIF-1α by inhibiting proteasomal degradation, leading to sustained VEGF expression and robust angiogenesis in vitro and in vivo. Taken together, these findings suggest that short proline-rich peptides can engage SH3 domains intracellularly and modulate cell signaling pathways. Indeed, the nanomolar-to-micromolar activity of BPC-157 observed in preclinical cellular assays raises the possibility of similar SH3 domain-mediated engagement; however, its intracellular trafficking, kinetic profile, and subcellular localization remain undefined and warrant further investigation.

At 15-amino acids, BPC-157 exceeds the typical substrate length for proton-coupled peptide transporters, and no receptor has been identified [*2,3*]. Nevertheless, by analogy to PR-39, it remains plausible that BPC-157 engages multiple surface components, such as integrins, heparan sulfate proteoglycans, or a yet unidentified receptor, to facilitate internalization via dynamin-dependent pathways [*65,87*]. As mentioned in Section 1.1, Hsieh et al. [*4*] demonstrated that dynasore, a dynamin inhibitor, blocks BPC-157–induced VEGFR2 internalization and signaling. However, because dynasore broadly inhibits both clathrin- and caveolin-mediated uptake [*88*], these findings indicate that endocytosis in general is essential for BPC-157 activity. As discussed in Section 1.2, VEGFR2 can signal ligand-independently through SFK transactivation, which drives clathrin-mediated endocytosis to initiate PI3K–Akt and ERK signaling from internalized endosomes [*29,52*]. Such a pathway may underlie BPC-157's activation of VEGFR2 signaling in a VEGFA-independent manner, requiring endocytic machinery for the peptide to first engage SFK SH3 domains to transactivate VEGF2R.

The computational workflow—comprising OmegaFold for de novo peptide structural modeling, DynamicBind for generating biochemically plausible binding orientations, and ICn3D for browser-based interaction analysis—provides an intuitive, modular pipeline for peptide modeling, docking, and residue-level contact assessment. Furthermore, the ability to recapitulate the canonical SH2-linker interaction with the c-Src SH3 domain in its autoinhibited conformation lends credibility to the predicted binding poses. Docking analyses were conducted using an earlier release of DynamicBind (v1.0), which accepted OmegaFold-derived PDB files as ligand inputs. In contrast, current versions available through the Neurosnap platform require SDF file ligand inputs, introducing slight algorithmic and conformer-sampling differences. To ensure transparency and reproducibility, the binding model results are provided in Supplementary Files S7–S10, with archived job links included in Supplementary File 31. The

reported interaction score offers a quantitative metric but should be interpreted as a structural hypothesis rather than a direct measure of binding affinity. Moreover, SH3 domain engagement represents only one potential route to SFK activation; alternative mechanisms include high-affinity extracellular receptor binding or modulation of Csk activity.

An important future consideration is how BPC-157 differentially engages ERK and Akt pathways in regenerative versus oncogenic contexts. As noted in Section 1.1, BPC-157 promotes cytoprotective and pro-growth signaling following injury, supporting tissue survival and repair. However, Skiret et al. [*21*] demonstrated that BPC-157 suppressed VEGF-driven MAPK/ERK activation and growth in melanoma cells, suggesting a selective inhibition of malignant signaling. This context-dependent regulation extends to angiogenesis: in the chick chorioallantoic membrane (CAM) assay, BPC-157 consistently enhanced vascular branching and density, reflecting pro-angiogenic activity via VEGFR2 signaling and endothelial migration [*4*]. In contrast, in corneal perforation models, BPC-157 accelerated epithelial repair while attenuating pathological neovascularization, thereby maintaining tissue integrity without promoting excessive vessel invasion [*83*]. Together, these findings underscore BPC-157's dual capacity to stimulate angiogenesis where physiologically beneficial, yet restrain aberrant vascular growth in tissues where neovascularization is detrimental, such as the eye. This selective regulation highlights BPC-157's potential as a therapeutic agent uniquely capable of balancing regenerative repair with oncogenic transformation.

Figure 5 provides strong evidence for robust intracellular expression of mCherry–BPC157$_2$, demonstrated by fluorescent imaging and immunoblot analysis of Sf9 manufacturing cell cultures. Because the culture supernatant was discarded prior to analysis, these data reflect intracellular protein levels and associated production products rather than the abundance or composition of secreted forms. The fusion construct includes an N-terminal insect cell-specific secretion signal peptide (22 amino acids; see Section 4.1), intentionally incorporated to facilitate extracellular export. Accordingly, future analysis of the culture supernatant will be essential to fully characterize secreted mCherry–BPC157$_2$ and evaluate the efficiency of post-translational processing.

Immunoblot signals at ~29 kDa (single-tail mCherry–BPC157) and ~26.6 kDa (mCherry domain) correspond to truncated fragments or pre-processed intermediates of fusion protein. The ~85 kDa band witnessed was absent in negative controls and consistent with SDS-resistant oligomerization or possible membrane-associated complexes. Together, these findings validate

the production of a fluorescent fusion protein incorporating C-terminal BPC-157 repeat sequences, establishing a platform for subsequent interaction analysis and localization studies.

Future work will focus on purification and functional validation. Affinity-based strategies, such as mCherry- or BPC-157-specific antibody bead capture or column chromatography can facilitate recovery of the fusion protein from cell culture supernatant. To confirm mCherry–$BPC157_2$ recapitulates the biological activity of monomeric BPC-157, phosphorylation assays targeting SFKs, FAK, ERK, and Akt should be initially incorporated to validate target pathway engagement.

In summary, the proposed model of BPC-157 as an SH3 domain–binding peptide provides a unifying framework linking BPC-157–induced pro-repair effects to SFK activation and downstream ERK/Akt signaling. The mCherry–$BPC157_2$ fusion protein represents a powerful experimental tool to interrogate this mechanism across biochemical and cellular models. Future studies aimed at elucidating the precise molecular mechanism of action, identifying potential receptors, and defining the potential intracellular activity of BPC-157 will be critical for clinical translation.

4.0
Materials and Methods

4.1.1
Fusion Protein Construction

A modular fusion protein was designed to incorporate a cleavable secretion signal, a fluorescent reporter, structured linkers, and tandem repeats of the therapeutic peptide BPC-157. The N-terminal domain consisted of mCherry, a red fluorescent protein chosen for its high photostability, monomeric nature, FRET compatibility, and reliable performance in fusion constructs [*89*]. To facilitate secretion in insect cells, the native start codon of mCherry was replaced with the melittin signal peptide from *Apis mellifera*, which directs co-translational translocation into the endoplasmic reticulum and is subsequently cleaved, enabling secretion of the processed protein into the culture medium during expression [*90*]. A rigid α-helical linker was positioned between mCherry and the therapeutic segment to maintain domain independence, reduce steric hindrance, and support proper folding of both domains [*91*]. The C-terminal region comprised two tandem repeats of BPC-157, separated by a flexible glycine–serine linker to improve solubility and provide conformational flexibility, potentially enhancing target engagement. Both nucleotide and amino acid sequences are provided in FASTA format in Supplementary File S25.

4.1.2
Docking Simulation Overview

To assess the potential of BPC-157 to adopt biochemically relevant orientations within SH3 domains, both BPC-157 and a 15-residue autoinhibitory SH2–linker peptide from c-Src (*NVCPTSKPQTQGLAK*; residues 243–257; UniProt ID: P00523) were modeled using OmegaFold v2 (released December, 2022) [*92,93,103*]. Predicted peptide structures were exported in PDB format. The resulting PDB files were docked to representative SH3 domain crystal structures using DynamicBind v1.0 (December, 2023) [*94,95*], and docking outputs were validated and analyzed in iCn3D v3.45.3 (September, 2025) [*96,97*]. Structural PDB files for SH3 domains were obtained directly from the RCSB Protein Data Bank and are provided in Supplementary Files S1-S3.

4.1.3

Structure Prediction and Visualization

The sequences of BPC-157 (*GEPPPGKPADDAGLV*) and the c-Src SH2–linker region (*NVCPTSKPQTQGLAK*; residues 243–257; UniProt ID: P00523) were submitted individually to OmegaFold (Model version 2, 10 cycles) for de novo folding [*92,93*]. Resulting 3D models were exported in PDB format for subsequent docking analyses. The full translated sequence of the processed mCherry–BPC157$_2$ fusion protein was submitted to IntelliFold (AlphaFold 3) [*98,99*]. Model #1 was selected using the following parameters: MSA mode = mmseqs2_uniref_env, no custom MSA, six recycles, 205 sampling steps, and five diffusion samples. SH3 binding models were visualized and annotated in iCn3D, while three-dimensional structures of BPC-157 and the fusion protein were rendered in the RCSB Mol* Viewer [*100,101*]. Atomic coordinates and PDB files of the modeled peptides, together with the PDB file of mCherry–BPC157$_2$, are provided in Supplementary Files S4–S6.

4.1.4
Peptide–SH3 Domain Docking

DynamicBind [*94,95*], a deep learning–based docking platform, was used to predict binding conformations between peptide ligands and SH3 domains. Input ligand structures for BPC-157 and the SH2–linker control were generated with OmegaFold in PDB format. SH3 domain structures were retrieved from the Protein Data Bank [*101*] (PDB IDs: 1SRL for c-Src, 1NYF for Fyn, 2HDA for Yes). Docking was performed with the following parameters: interference steps = 20, Model Version 2, Relax Structure and Noise options enabled, and random seed = 20. The top 10 ranked conformations were analyzed in iCn3D. Specific models selected for detailed analysis were: Rank 1 (c-Src SH2–linker control), Rank 3 (c-Src–BPC-157), Rank 2 (Fyn–BPC-157), and Rank 10 (Yes–BPC-157), corresponding to Supplementary Files S7–S10.

All docking analyses were performed using an earlier version of DynamicBind (v1.0 December 2023, GitHub: https://github.com/luwei0917/DynamicBind) that accepted peptide ligands directly in PDB format, with atomic coordinates used as the basis for docking. Current builds of DynamicBind accessed through the Neurosnap platform require ligands to be supplied in SDF format, which are parsed as chemical graphs rather than raw coordinates. As a result, even when the same peptide structure is converted from PDB to SDF, the conformer ensemble generated by DynamicBind differs slightly from that produced in earlier runs when using the Neurosnap interface. To ensure transparency, all original PDB-based jobs and outputs are archived on the Neurosnap website (*Supplementary File S31*), and the outputs from the original

DynamicBind runs are provided as Supplementary Files S7–S10. Converted SDF files generated from OmegaFold PDB outputs are provided in Supplementary Files S29 and S30. Please note that SDF input files were not used for analysis for this manuscript. Full completed DynamicBind jobs are archived as Supplementary Files S32-S35.

4.1.5
Interaction Analysis

Supplementary Files S11–S14 contain ICn3D PNG state files, which can be reopened directly in ICn3D with the interaction analyses pre-computed. Predicted peptide–protein complexes (*Supplementary Files S7-S10*) were imported into iCn3D (version 3.45.3; build date: September, 2025) [*96,97*] for interaction mapping. Contacts were defined as follows: hydrogen bonds (≤ 3.8 Å), salt bridges (≤ 6.0 Å), hydrophobic contacts (≤ 4.0 Å), and π-stacking interactions (≤ 5.5 Å). Interaction maps were generated using the “Analysis” tab, with receptor and ligand specified in designated boxes. For comparative analysis, an interaction score (IS) was calculated using a weighted heuristic: π–π stacking (+3), cation–π (+4), hydrogen bonds (+5) [*84–86*]. This metric was used to highlight stabilizing features rather than absolute binding energies. Control docking of the c-Src SH2–linker to its SH3 domain was included for reference. Results and Interaction Analysis are summarized in Figure 4 and Table 1 and provided as a PDF and XLSX in Supplementary Files S15 and S16.

4.1.6
Mechanistic Model Construction

Mechanistic diagrams depicting BPC-157–induced signaling pathways and SH3-mediated activation of Src family kinases were constructed based on published literature. Modeled pathways included Src–Caveolin–eNOS, Src–FAK, Src–Akt, and FAK–Akt. These diagrams integrate current understanding of SFK regulation, SH2/SH3 autoinhibition, caveolin-dependent eNOS repression, and angiogenic signaling cascades triggered by BPC-157 [*2–8,11,24,33,35,42,50,51*]. Figures were generated using Google Draw (Google LLC, Mountain View, CA, USA) and PicsArt (PicsArt LLC, Miami, FL, USA).

4.1.7
Fusion Protein Sequences

The coding sequence for the mCherry–BPC157$_2$ fusion protein was codon-optimized for

Spodoptera frugiperda (Sf9) expression using the VectorBuilder Online Design Studio (VectorBee, VectorBuilder, Chicago, IL, USA). Both nucleotide and amino acid sequences are provided in FASTA format in Supplementary File S25.

4.1.8

Baculovirus and Protein Expression Vector Construction

A custom recombinant baculovirus expression vector encoding the mCherry–$BPC157_2$ fusion construct was designed by the author and synthesized by VectorBuilder (Chicago, IL, USA). The open reading frame (ORF) was placed under the control of the *Autographa californica* multiple nucleopolyhedrovirus polyhedrin promoter to drive high-level expression. A Simian Virus 40 early polyadenylation signal was included downstream of the ORF to ensure efficient transcriptional termination. The transfer vector incorporated Tn7 left and right terminal elements for site-specific transposition into a bacmid attTn7 site in the presence of Tn7 transposase. For propagation and selection in *E. coli*, the plasmid contained an ampicillin resistance gene and a pUC origin of replication. A gentamicin resistance marker enabled selection of recombinant bacmid clones following transposition. Vector design was managed through VectorBuilder's online platform (https://en.vectorbuilder.com/design/pBV.html).

4.1.9

Generation of Recombinant Baculovirus and Fluorescent Imaging

A custom recombinant baculovirus encoding the mCherry–$BPC157_2$ fusion construct was generated by VectorBuilder (Chicago, IL, USA) using a bacmid shuttle vector system. Briefly, bacmid DNA was transfected into Sf9 cells to produce viral particles, which were amplified through multiple infection rounds to obtain high-titer stocks [*90,102*]. During amplification, Sf9 cells were infected and imaged daily over a 7-day period using brightfield and epifluorescence microscopy to monitor mCherry expression. Imaging was performed on an Olympus IX73 laser scanning confocal microscope equipped with an Hg arc lamp (530–550 nm excitation) and a TRITC/mCherry filter set. Images were acquired at 100× total magnification (objective 10×, eyepiece 10×). Red channel exposure times were 80 ms on days 1, 2, and 4, and 10 ms on day 7. Brightfield images from days 4 and 7 were uniformly adjusted for brightness and contrast to compensate for inter-day exposure variation. All unprocessed image files are provided in Supplementary Files S17–S24.

4.2.0

Sf9 Cell Culture, Infection, Protein Expression

Sf9 insect cells (Expression Systems, Davis, CA, USA) were cultured in ESF921 medium (Expression Systems, Davis, CA, USA) at 28 °C in a T75 flask (Thermo Scientific, Waltham, MA, USA). Upon reaching a density of approximately 5×10^6 cells per flask, recombinant custom baculovirus (VectorBuilder, Chicago, IL, USA) was added at a multiplicity of infection (MOI) of 2. After 48 hours, the culture medium was replaced. At 120 hours post-infection, cells were harvested by centrifugation at 400 × g for 10 minutes, washed once with fresh ESF921 medium, and centrifuged again under the same conditions. The supernatant was discarded, and the resulting cell pellet was briefly air-dried before flash-freezing in a dry ice–isopropanol (99%) bath.

4.2.1

Western Blot Analysis

Western blotting was conducted by Boster Bio (Pleasanton, CA, USA). Frozen pellets of transduced Sf9 cells were lysed, denatured, and separated on 4–12% Bis-Tris Plus gel (Thermo Scientific, Waltham, MA, USA), with protein loading standardized to 10 µg per lane. Proteins were transferred to PVDF membranes using Tris-Glycine buffer overnight. Membranes were incubated for 16 h at 8 °C with a rabbit polyclonal anti-mCherry antibody (Abcam ab167453) diluted 1:1000. Detection was performed using fluorophore-conjugated secondary antibodies, and imaging was carried out with the Odyssey CLx fluorescent imaging system. Supporting controls, including a secondary-only blot, original blot image, BCA assay (Thermo Scientific, Waltham, MA, USA) protein concentration determination, and a replicate probed at 1:500, are provided in Supplementary Files S26-S8.

**All data supporting the conclusions of this study are included in the article and its supplementary information files. Supplementary Files are also available online at: https://drive.google.com/drive/folders/1bdzCHSisj9Z3uyCRy8uYnSJM032ccIq6*

5.0
Declaration and Acknowledgments

5.1
Declaration of generative AI and AI-assisted technologies in the writing process

During the preparation of this work, the author utilized Perplexity.ai (AI Chatbot, Large Language Model, https://www.perplexity.ai/) and Microsoft Copilot (AI Companion powered by GPT-5) to assist in formatting original writing to meet scientific peer-reviewed standards. All content was subsequently reviewed and edited by the author, who takes full responsibility for the final published version.

5.2
Funding

This research did not receive any specific grant from funding agencies in the public, commercial, or not-for-profit sectors.

5.3
Competing Interest Statement

Steven Schlosser is the CEO of Cell Shot Nutrition. This company does not manufacture or market products related to the subject of this manuscript.

5.4
Acknowledgments

I would like to sincerely thank my parents, Steve and Evelyn, and my cats, Bear and Mr. P, for their unwavering support and companionship. I dedicate this work to the memory of Professor Roland Wolkowicz (1962–2020), whose teachings continue to guide me.

REFERENCES

[1] Sikirić, P., Petek, M., Ručman, R., Seiwerth, S., Grabarević, Z., Rotkvić, I., Turković, B., Jagić, V., Mildner, B., Duvnjak, M., Lang, N., Danilović, Z., Cviko, A., Kolega, M., Sallmani, A., Djačić, S., Bura, M., Brkić, T., Banić, M., … Karakas, I. (1993). A new gastric juice peptide, BPC. An overview of the stomach-stress-organoprotection hypothesis and beneficial effects of BPC. *Journal of Physiology-Paris, 87*(5), 313–327. https://doi.org/10.1016/0928-4257(93)90038-U

[2] Vasireddi, N., Hahamyan, H., Salata, M. J., Karns, M., Calcei, J. G., Voos, J. E., & Apostolakos, J. M. (2025). Emerging use of BPC-157 in orthopaedic sports medicine: A systematic review. *HSS Journal*. https://doi.org/10.1177/15563316251355551

[3] McGuire, F. P., Martinez, R., Lenz, A., et al. (2025). Regeneration or risk? A narrative review of BPC-157 for musculoskeletal healing. *Current Reviews in Musculoskeletal Medicine, 18*, 611–619. https://doi.org/10.1007/s12178-025-09990-7

[4] Hsieh, M. J., Liu, H. T., Wang, C. N., Huang, H. Y., Lin, Y., Ko, Y. S., … Pang, J. H. S. (2017). Therapeutic potential of pro-angiogenic BPC157 is associated with VEGFR2 activation and up-regulation. *Journal of Molecular Medicine, 95*(3), 323–333. https://doi.org/10.1007/s00109-016-1488-y

[5] Hsieh, M. J., Lee, C. H., Chueh, H. Y., Chang, G. J., Huang, H. Y., Lin, Y., & Pang, J. H. S. (2020). Modulatory effects of BPC 157 on vasomotor tone and the activation of Src-Caveolin-1-endothelial nitric oxide synthase pathway. *Scientific Reports, 10*(1), 17078. https://doi.org/10.1038/s41598-020-74022-y

[6] Chang, C. H., Tsai, W. C., Lin, M. S., Hsu, Y. H., & Pang, J. H. S. (2011). The promoting effect of pentadecapeptide BPC 157 on tendon healing involves tendon outgrowth, cell survival, and cell migration. *Journal of Applied Physiology, 110*(3), 774–780. https://doi.org/10.1152/japplphysiol.00945.2010

[7] Chang, C. H., Tsai, W. C., Hsu, Y. H., & Pang, J. H. S. (2014). Pentadecapeptide BPC 157 enhances growth hormone receptor expression in tendon fibroblasts. *Molecules, 19*(11), 19066–19077. https://doi.org/10.3390/molecules191119066

[8] Huang, T., Zhang, K., Sun, L., Xue, X., Zhang, C., Shu, Z., … Zhang, W. (2015). Body protective compound-157 enhances alkali-burn wound healing in vivo and promotes proliferation, migration, and angiogenesis in vitro. *Drug Design, Development and Therapy, 9*, 2485–2499. https://doi.org/10.2147/DDDT.S82030

[9] Seiwerth, S., Milavic, M., Vukojevic, J., Gojkovic, S., Krezic, I., Vuletic, L. B., … Sikiric, P. (2021). Stable gastric pentadecapeptide BPC 157 and wound healing. *Frontiers in Pharmacology, 12*, 627533. https://doi.org/10.3389/fphar.2021.627533

[10] Wang, S. H., Lin, L. P., Lin, M. S., Pang, J. H. S., & Tsai, W. C. (2019). BPC 157 promotes skeletal muscle cells migration in association with up-regulation of paxillin and vinculin expression. *Rehabilitation Practice and Science, 47*(1), 21–29. https://doi.org/10.6315/TJPMR.201906_47(1).0003

[11] Kim, L. C., Song, L., & Haura, E. B. (2009). Src kinases as therapeutic targets for cancer. *Nature Reviews Clinical Oncology, 6*(10), 587–595. https://doi.org/10.1038/nrclinonc.2009.129

[12] Sirvent, A., Mevizou, R., Naim, D., Lafitte, M., & Roche, S. (2020). Src Family Tyrosine Kinases in Intestinal Homeostasis, Regeneration and Tumorigenesis. *Cancers, 12*(8), 2014. https://doi.org/10.3390/cancers12082014

[13] Ortiz, M. A., Mikhailova, T., Li, X., Porter, B. A., Bah, A., & Kotula, L. (2021). Src family kinases, adaptor proteins and the actin cytoskeleton in epithelial-to-mesenchymal transition. *Cell Communication and Signaling, 19*(1), 67. https://doi.org/10.1186/s12964-021-00750-x

[14] Skorjanec, S., Kokot, A., Drmic, D., Radic, B., Sever, M., Klicek, R., Kolenc, D., Zenko, A., Lovric Bencic, M., Belosic Halle, Z., Situm, A., Zivanovic Posilovic, G., Masnec, S., Suran, J., Aralica, G., Seiwerth, S., & Sikiric, P. (2015). Duodenocutaneous fistula in rats as a model for "wound healing-therapy" in ulcer healing: The effect of pentadecapeptide BPC 157, L-nitro-arginine methyl ester and L-arginine. *Journal of Physiology and Pharmacology, 66*(4), 581–590. https://pubmed.ncbi.nlm.nih.gov/26348082/

[15] Klicek, R., Kolenc, D., Šuran, J., Drmić, D., Brčić, L., Aralica, G., Sever, M., Holjevac, J., Radić, B., Turudić, T., Kokot, A., Patrlj, L., Ručman, R., Seiwerth, S., & Sikiric, P. (2013). Stable gastric

pentadecapeptide BPC 157 heals cysteamine-colitis and colon-colon-anastomosis and counteracts cuprizone brain injuries and motor disability. *Journal of Physiology and Pharmacology, 64*(5), 597–612. https://pubmed.ncbi.nlm.nih.gov/24304574

[16] Vukojević, J., Vrdoljak, B., Malekinušić, D., Siroglavić, M., Milavić, M., Kolenc, D., … Sikiric, P. (2020). The effect of pentadecapeptide BPC 157 on hippocampal ischemia/reperfusion injuries in rats. *Brain and Behavior, 10*(8), e01726. https://doi.org/10.1002/brb3.1726

[17] Perovic, D., Milavic, M., Dokuzovic, S., Krezic, I., Gojkovic, S., Vranes, H., … Sikiric, P. (2022). Novel therapeutic effects in rat spinal cord injuries: Recovery of the definitive and early spinal cord injury by the administration of pentadecapeptide BPC 157 therapy. *Current Issues in Molecular Biology, 44*(5), 1901–1927. https://doi.org/10.3390/cimb44050130

[18] Cerovecki, T., Bojanic, I., Brcic, L., Radic, B., Vukoja, I., Seiwerth, S., & Sikiric, P. (2010). Pentadecapeptide BPC 157 (PL 14736) improves ligament healing in the rat. *Journal of Orthopaedic Research, 28*(9), 1155–1161. https://doi.org/10.1002/jor.21107

[19] Staresinic, M., Sebecic, B., Patrlj, L., Jadrijevic, S., Suknaic, S., Perovic, D., Aralica, G., Zarkovic, N., Borovic, S., Srdjak, M., Hajdarevic, K., Kopljar, M., Batelja, L., Boban-Blagaic, A., Turcic, I., Anic, T., Seiwerth, S., & Sikiric, P. (2003). Gastric pentadecapeptide BPC 157 accelerates healing of transected rat Achilles tendon and in vitro stimulates tendocytes growth. *Journal of Orthopaedic Research, 21*(6), 976–983. https://doi.org/10.1016/S0736-0266(03)00110-4

[20] Guo, Y. J., Pan, W. W., Liu, S. B., Shen, Z. F., Xu, Y., & Hu, L. L. (2020). ERK/MAPK signalling pathway and tumorigenesis. *Experimental and Therapeutic Medicine, 19*(3), 1997–2007. https://doi.org/10.3892/etm.2020.8454

[21] Radeljak, S., Seiwerth, S., & Sikiric, P. (2004). BPC 157 inhibits cell growth and VEGF signalling via the MAPK kinase pathway in the human melanoma cell line. *Melanoma Research, 14*(4), A14–A15.

[22] Wan, Q., Truong Vo, T., Steele, H. E., Ozcelikkale, A., Han, B., Wang, Y., Oh, J., Yokota, H., & Na, S. (2017). Subcellular domain-dependent molecular hierarchy of SFK and FAK in mechanotransduction and cytokine signaling. *Scientific Reports, 7*(1), Article 9033. https://doi.org/10.1038/s41598-017-09495-5

[23] Khatun, Z., Saikat, S., & Haque, S. (2025). Src family kinases in epidermal homeostasis, wound healing, and tumorigenesis. *Journal of Biosciences and Public Health, 1*(2), 17–26. https://doi.org/10.5455/JBPH.2025.08

[24] Bolós, V., Gasent, J. M., López-Tarruella, S., & Grande, E. (2010). The dual kinase complex FAK-Src as a promising therapeutic target in cancer. *OncoTargets and Therapy, 3*, 83–97. https://doi.org/10.2147/OTT.S6909

[25] Karar, J., & Maity, A. (2011). PI3K/AKT/mTOR pathway in angiogenesis. *Frontiers in Molecular Neuroscience, 4*, 51. https://doi.org/10.3389/fnmol.2011.00051

[26] Kaidi, A., Williams, A. C., & Paraskeva, C. (2006). Direct transcriptional up-regulation of cyclooxygenase-2 by hypoxia-inducible factor-1 promotes colorectal tumor cell survival. *Cancer Research, 66*(13), 6683–6691. https://doi.org/10.1158/0008-5472.CAN-06-0425

[27] Treisman, R. (1996). Regulation of transcription by MAP kinase cascades. *Current Opinion in Cell Biology, 8*(2), 205–215. https://doi.org/10.1016/S0955-0674(96)80067-6

[28] Hausott, B., & Klimaschewski, L. (2019). Promotion of peripheral nerve regeneration by stimulation of the extracellular signal-regulated kinase (ERK) pathway. *Anatomical Record, 302*(8), 1261–1267. https://doi.org/10.1002/ar.24126

[29] Wu, X., Yang, L., Zheng, Z., Li, Z., Shi, J., Li, Y., … Hu, D. (2016). Src promotes cutaneous wound healing by regulating MMP-2 through the ERK pathway. *International Journal of Molecular Medicine, 37*(3), 639–648. https://doi.org/10.3892/ijmm.2016.2472

[30] Lee, S., Kim, M. S., Jung, S. J., et al. (2018). ERK activating peptide, AES16-2M, promotes wound healing through accelerating migration of keratinocytes. *Scientific Reports, 8*, 14398. https://doi.org/10.1038/s41598-018-32851-y

[31] Encinas, M., Tansey, M. G., Tsui-Pierchala, B. A., Comella, J. X., Milbrandt, J., & Johnson Jr, E. M. (2001). c-Src is required for glial cell line-derived neurotrophic factor (GDNF) family ligand-mediated neuronal survival via a phosphatidylinositol-3 kinase (PI-3K)-dependent pathway. *Journal of Neuroscience, 21*(5), 1464-1472. https://doi.org/10.1523/JNEUROSCI.21-05-01464.2001

[32] Jin, Z. G., Ueba, H., Tanimoto, T., Lungu, A. O., Frame, M. D., & Berk, B. C. (2003). Ligand-independent activation of vascular endothelial growth factor receptor 2 by fluid shear stress regulates activation of endothelial nitric oxide synthase. *Circulation Research, 93*(4), 354–363. https://doi.org/10.1161/01.RES.0000089257.94002.96

[33] Gates, A., Hohenester, S., Anwer, M. S., & Webster, C. R. (2009). cAMP-GEF cytoprotection by Src tyrosine kinase activation of phosphoinositide-3-kinase p110 beta/alpha in rat hepatocytes. *American Journal of Physiology-Gastrointestinal and Liver Physiology, 296*(4), G764–G774. https://doi.org/10.1152/ajpgi.90622.2008

[34] Phung, T. L., et al. (2006). Endothelial Akt1 mediates angiogenesis by phosphorylating multiple substrates including eNOS. *Proceedings of the National Academy of Sciences, 111*(13), 4823–4832. https://doi.org/10.1073/pnas.1408472111

[35] Fisslthaler, B., Dimmeler, S., Hermann, C., Busse, R., & Fleming, I. (2000). Phosphorylation and activation of the endothelial nitric oxide synthase by fluid shear stress. *Acta Physiologica Scandinavica, 168*(1), 81–88. https://doi.org/10.1046/j.1365-201x.2000.00627.x

[36] Chen, J., Crawford, R., Chen, C., & Xiao, Y. (2013). The key regulatory roles of the PI3K/Akt signaling pathway in the functionalities of mesenchymal stem cells and applications in tissue regeneration. *Tissue Engineering Part B: Reviews, 19*(6), 516–528. https://doi.org/10.1089/ten.teb.2012.0672

[37] Shiojima, I., & Walsh, K. (2002). Role of Akt signaling in vascular homeostasis and angiogenesis. *Circulation Research, 90*(12), 1243–1250. https://doi.org/10.1161/01.RES.0000022200.71892.9F

[38] Datta, K., Bellacosa, A., Chan, T. O., & Tsichlis, P. N. (1996). Akt is a direct target of the phosphatidylinositol 3-kinase: Activation by growth factors, v-src and v-Ha-ras, in Sf9 and mammalian cells. *Journal of Biological Chemistry, 271*(48), 30835–30839. https://doi.org/10.1074/jbc.271.48.30835

[39] Andrabi, S. M., Sharma, N. S., Karan, A., Shahriar, S. M. S., Cordon, B., Ma, B., & Xie, J. (2023). Nitric oxide: Physiological functions, delivery, and biomedical applications. *Advanced Science (Weinh), 10*(30), e2303259. https://doi.org/10.1002/advs.202303259

[40] Yeatman, T. A renaissance for SRC. *Nat Rev Cancer 4*, 470–480 (2004). https://doi.org/10.1038/nrc1366

[41] Matrone, C., Petrillo, F., Nasso, R., & Ferretti, G. (2020). Fyn tyrosine kinase as harmonizing factor in neuronal functions and dysfunctions. International Journal of Molecular Sciences, 21(12), 4444. https://doi.org/10.3390/ijms21124444

[42] Jin, Y., Ding, Y., Richards, M., Kaakinen, M., Giese, W., Baumann, E., Szymborska, A., Rosa, A., Nordling, S., Schimmel, L., Akmeriç, E. B., Pena, A., Nwadozi, E., Jamalpour, M., Holstein, K., Sáinz-Jaspeado, M., Bernabeu, M. O., Welsh, M., Gordon, E., Franco, C. A., Vestweber, D., Eklund, L., Gerhardt, H., & Claesson-Welsh, L. (2022). Tyrosine-protein kinase Yes controls endothelial junctional plasticity and barrier integrity by regulating VE-cadherin phosphorylation and endocytosis. *Nature Cardiovascular Research, 1*(12), 1156–1173. https://doi.org/10.1038/s44161-022-00172-z

[43] Selzer, A. M., et al. (2024). Small-molecule allosteric modulators of the AML-associated Src-family kinase, Hck. *Biophysical Journal, 123*(3), 185a. https://doi.org/10.1016/j.bpj.2022.11.1057

[44] Boggon, T. J., & Eck, M. J. (2004). Structure and regulation of Src family kinases. *Oncogene, 23*(48), 7918–7927. https://doi.org/10.1038/sj.onc.1208081

[45] Shenoy-Scaria, A. M., et al. (1994). Cysteine 3 of Src family protein tyrosine kinase determines palmitoylation and localization in caveolae. *The Journal of Cell Biology, 126*(2), 353–363. https://doi.org/10.1083/jcb.126.2.353

[46] Maniatis, N. A., Brovkovych, V., Allen, S. E., John, T. A., Shajahan, A. N., Tiruppathi, C., Vogel, S. M., Skidgel, R. A., Malik, A. B., & Minshall, R. D. (2006). Novel mechanism of endothelial nitric oxide synthase activation mediated by caveolae internalization in endothelial cells. *Circulation Research, 99*(8), 870–877. https://doi.org/10.1161/01.RES.0000245187.08026.47

[47] Okamoto, T., Schlegel, A., Scherer, P. E., & Lisanti, M. P. (1998). Caveolins, a family of scaffolding proteins for organizing "preassembled signaling complexes" at the plasma membrane. *Journal of Biological Chemistry, 273*(10), 5419-5422. https://doi.org/10.1074/jbc.273.10.5419

[48] Fulton, D., Church, J. E., Ruan, L., Li, C., Sood, S. G., Kemp, B. E., Jennings, I. G., & Venema, R. C. (2005). Src kinase activates endothelial nitric-oxide synthase by phosphorylating Tyr-83*. *Journal of Biological Chemistry, 280*(43), 35943–35952. https://doi.org/10.1074/jbc.M504606200

[49] Tahir, S. A., Park, S., & Thompson, T. C. (2009). Caveolin-1 regulates VEGF-stimulated angiogenic activities in prostate cancer and endothelial cells. *Cancer Biology & Therapy, 8*(23), 2284–2294. https://doi.org/10.4161/cbt.8.23.10138

[50] Li, S., Couet, J., & Lisanti, M. P. (1996). Src tyrosine kinases, Galpha subunits, and H-Ras share a common membrane-anchored scaffolding protein, caveolin. Caveolin binding negatively regulates the auto-activation of Src tyrosine kinases. *Journal of Biological Chemistry, 271*(46), 29182–29190. https://doi.org/10.1074/jbc.271.46.29182

[51] Saxena, M., Liu, S., Yang, B., Hajal, C., Changede, R., Hu, J., Wolfenson, H., Hone, J., & Sheetz, M. P. (2017). EGFR and HER2 activate rigidity sensing only on rigid matrices. *Nature Materials, 16*(7), 775–781. https://doi.org/10.1038/nmat4893

[52] Simons, M., Gordon, E., & Claesson-Welsh, L. (2016). Mechanisms and regulation of endothelial VEGF receptor signalling. *Nature Reviews Molecular Cell Biology, 17*(10), 611–625. https://doi.org/10.1038/nrm.2016.87

[53] Boczek, E. E., Luo, Q., Dehling, M., Röpke, M., Mader, S. L., Seidl, A., Kaila, V. R. I., & Buchner, J. (2019). Autophosphorylation activates c-Src kinase through global structural rearrangements. *Journal of Biological Chemistry, 294*(35), 13186–13197. https://doi.org/10.1074/jbc.RA119.008199

[54] Xu, W., Harrison, S. C., & Eck, M. J. (1997). Three-dimensional structure of the tyrosine kinase c-Src. *Nature, 385*(6617), 595–602. https://doi.org/10.1038/385595a0

[55] Moroco, J. A., Craigo, J. K., Iacob, R. E., Wales, T. E., Engen, J. R., & Smithgall, T. E. (2014). Differential sensitivity of Src-family kinases to activation by SH3 domain displacement. *PLoS ONE, 9*(8), e105629. https://doi.org/10.1371/journal.pone.0105629

[56] Yadav, S. S., & Miller, W. T. (2007). Cooperative activation of Src family kinases by SH3 and SH2 ligands. *Cancer Letters, 257*(2), 163–170. https://doi.org/10.1016/j.canlet.2007.07.012

[57] Pakharukova, N., Thomas, B. N., Bansia, H., Li, L., Abzalimov, R. R., Kim, J., Kahsai, A. W., Pani, B., Bassford, D. K., Liu, S., Zhang, X., des Georges, A., & Lefkowitz, R. J. (2025). Mechanism of beta-arrestin 1 mediated Src activation via Src SH3 domain revealed by cryo-electron microscopy [Preprint]. *bioRxiv*. https://doi.org/10.1101/2024.07.31.605623

[58] Pellicena, P., & Miller, W. T. (2001). Processive phosphorylation of p130Cas by Src depends on SH3-polyproline interactions. *Journal of Biological Chemistry, 276*(30), 28190–28196. https://doi.org/10.1074/jbc.M100055200

[59] Daday, C., de Buhr, S., Mercadante, D., & Gräter, F. (2022). Mechanical force can enhance c-Src kinase activity by impairing autoinhibition. *Biophysical Journal, 121*(5), 684–691. https://doi.org/10.1016/j.bpj.2022.01.028

[60] Lerner, E. C., & Smithgall, T. E. (2002). SH3-dependent stimulation of Src-family kinase autophosphorylation without tail release from the SH2 domain in vivo. *Nature Structural Biology, 9*(5), 365–369. https://doi.org/10.1038/nsb782

[61] Arias-Salgado, E. G., Lizano, S., Sarkar, S., Brugge, J. S., Ginsberg, M. H., & Shattil, S. J. (2003). Src kinase activation by direct interaction with the integrin β cytoplasmic domain. *Proceedings of the National Academy of Sciences, 100*(23), 13298–13302. https://doi.org/10.1073/pnas.2336149100

[62] Schaller, M. D., Hildebrand, J. D., & Parsons, J. T. (1999). Complex formation with focal adhesion kinase: A mechanism to regulate activity and subcellular localization of Src kinases. *Molecular Biology of the Cell, 10*(10), 3489–3505. https://doi.org/10.1091/mbc.10.10.3489

[63] Pereira, E. A., & da Silva, L. L. P. (2016). HIV-1 Nef: Taking control of protein trafficking. *Traffic, 17*(9), 976–996. https://doi.org/10.1111/tra.12412

[64] Trible, R. P., Emert-Sedlak, L., & Smithgall, T. E. (2006). HIV-1 Nef selectively activates Src family kinases Hck, Lyn, and c-Src through direct SH3 domain interaction. *Journal of Biological Chemistry, 281*(37), 27029–27038. https://doi.org/10.1074/jbc.M601128200

[65] Chan, Y. R., Chen, C. L., Yu, C., & Luftig, R. B. (1998). PR-39, a syndecan-inducing antimicrobial peptide, binds and affects p130Cas. *Journal of Biological Chemistry, 273*(44), 28978–28985. https://doi.org/10.1074/jbc.273.44.28978

[66] Okada, M. (2012). Regulation of the Src family kinases by Csk. *International Journal of Biological Sciences, 8*(10), 1385–1397. https://doi.org/10.7150/ijbs.5141

[67] Yu, H., Chen, J. K., Feng, S., Dalgarno, D. C., Brauer, A. W., & Schreiber, S. L. (1994). Structural basis for the binding of proline-rich peptides to SH3 domains. *Cell, 76*(5), 933–945. https://doi.org/10.1016/0092-8674(94)90367-0

[68] Mayer, B. J., & Baltimore, D. (1993). Signalling through SH2 and SH3 domains. *Trends in Cell Biology, 3*(1), 8–13. https://doi.org/10.1016/0962-8924(93)90194-6

[69] Lee, C. H., Leung, B., Lemmon, M. A., Zheng, J., Cowburn, D., Kuriyan, J., & Saksela, K. (1995). A single amino acid in the SH3 domain of Hck determines its high affinity and specificity in binding to HIV-1 Nef protein. *EMBO Journal, 14*(20), 5006–5015. https://doi.org/10.1002/j.1460-2075.1995.tb00183.x

[70] Kurochkina, N., & Guha, U. (2013). SH3 domains: Modules of protein–protein interactions. *Biophysical Reviews, 5*(1), 29–39. https://doi.org/10.1007/s12551-012-0081-z

[71] Alexandropoulos, K., Cheng, G., & Baltimore, D. (1995). Proline-rich sequences that bind to Src homology 3 domains with individual specificities. Proceedings of the National Academy of *Sciences, 92*(8), 3110–3114. https://doi.org/10.1073/pnas.92.8.3110

[72] Mehrabipour, M., Jasemi, N. S. K., Dvorsky, R., & Ahmadian, M. R. (2023). A systematic compilation of human SH3 domains: A versatile superfamily in cellular signaling. *Cells, 12*(16), 2054. https://doi.org/10.3390/cells12162054

[73] Kazlauskas, A., Schmotz, C., Kesti, T., Hepojoki, J., Kleino, I., Kaneko, T., … Saksela, K. (2016). Large-scale screening of preferred interactions of human Src homology-3 (SH3) domains using native target proteins as affinity ligands. *Molecular & Cellular Proteomics, 15*(10), 3270–3281. https://doi.org/10.1074/mcp.M116.060483

[74] Adzhubei, A. A., Sternberg, M. J. E., & Makarov, A. A. (2013). Polyproline-II helix in proteins: Structure and function. *Journal of Molecular Biology, 425*(12), 2104–2132. https://doi.org/10.1016/j.jmb.2013.03.018

[75] Saksela, K., & Permi, P. (2012). SH3 domain ligand binding: What's the consensus and where's the specificity? *FEBS Letters, 586*(17), 2609–2614. https://doi.org/10.1016/j.febslet.2012.04.042

[76] Sudol, M., & Hunter, T. (2000). WW and SH3 domains, two different scaffolds to recognize proline-rich ligands. *FEBS Letters, 492*(3), 133–138. https://doi.org/10.1016/S0014-5793(01)03290-2

[77] Ball, L. J., Jarchau, T., Oschkinat, H., & Walter, U. (2002). EVH1 domains: Structure, function and interactions. *FEBS Letters, 513*(1), 45–52. https://doi.org/10.1016/S0014-5793(01)03291-4

[78] Salinas-Garcia, M. C., Plaza-Garrido, M., & Camara-Artigas, A. (2021). The impact of oncogenic mutations of the viral Src kinase on the structure and stability of the SH3 domain. Acta Crystallographica Section D: *Structural Biology, 77*(Pt 6), 854–866. https://doi.org/10.1107/S2059798321004344

[79] Williams, J. C., Wierenga, R. K., & Saraste, M. (1998). Insights into Src kinase functions: Structural comparisons. *Trends in Biochemical Sciences, 23*(5), 179–184. https://doi.org/10.1016/S0968-0004(98)01202-X

[80] Larson, S. M., & Davidson, A. R. (2000). The identification of conserved interactions within the SH3 domain by alignment of sequences and structures. *Protein Science, 9*(11), 2170–2180. https://doi.org/10.1110/ps.9.11.2170

[81] Hou, T., Chen, K., McLaughlin, W. A., Lu, B., & Wang, W. (2006). Computational analysis and prediction of the binding motif and protein interacting partners of the Abl SH3 domain. *PLoS Computational Biology, 2*(1), e1. https://doi.org/10.1371/journal.pcbi.0020001

[82] Li, J., Post, M., Volk, R., Gao, Y., Li, M., Metais, C., Sato, K., Tsai, J., Aird, W., Rosenberg, R. D., Hampton, T. G., Sellke, F., Carmeliet, P., & Simons, M. (2000). PR39, a peptide regulator of angiogenesis. *Nature Medicine, 6*(1), 49–55. https://doi.org/10.1038/71527

[83] Masnec, S., Kokot, A., Zlatar, M., Kalauz, M., Kunjko, K., Radic, B., Klicek, R., Drmic, D., Lazic, R., Brcic, L., Radic, R., Ivekovic, R., Seiwerth, S., & Sikiric, P. (2015). Perforating corneal injury in rat and pentadecapeptide BPC 157. *Experimental Eye Research, 136*, 9–15. https://doi.org/10.1016/j.exer.2015.04.016

[84] Hunter, C. A., & Sanders, J. K. M. (1990). The nature of π–π interactions. *Journal of the American Chemical Society, 112*(14), 5525–5534. https://doi.org/10.1021/ja00170a016

[85] Dougherty, D. A. (1996). Cation-π interactions in chemistry and biology: A new view of benzene, Phe, Tyr, and Trp. *Science, 271*(5246), 163–168. https://doi.org/10.1126/science.271.5246.163
[86] G.A. Jeffrey, Hydrogen Bonding in Biological Structures, Springer, Berlin, 1991. https://doi.org/10.1007/978-3-642-85135-3
[87] Doherty, G. J., & McMahon, H. T. (2009). Mechanisms of endocytosis. *Annual Review of Biochemistry, 78*, 857–902. https://doi.org/10.1146/annurev.biochem.78.081307.110540
[88] Kirchhausen, T., Macia, E., & Pelish, H. E. (2008). Use of dynasore, the small molecule inhibitor of dynamin, in the regulation of endocytosis. *Methods in Enzymology, 438*, 77–93. https://doi.org/10.1016/S0076-6879(07)38006-3
[89] Shaner, N. C., Campbell, R. E., Steinbach, P. A., Giepmans, B. N., Palmer, A. E., & Tsien, R. Y. (2004). Improved monomeric red, orange and yellow fluorescent proteins derived from Discosoma sp. red fluorescent protein. *Nature Biotechnology, 22*(12), 1567–1572. https://doi.org/10.1038/nbt1037
[90] Tessier, D. C., Thomas, D. Y., Khouri, H. E., Laliberté, F., & Vernet, T. (1991). Enhanced secretion from insect cells of a foreign protein fused to the honeybee melittin signal peptide. *Gene, 98*(2), 177–183. https://doi.org/10.1016/0378-1119(91)90171-7
[91] Li, G., Huang, Z., Zhang, C., Fang, M., Deng, H., & Wu, S. (2016). Construction of a linker library with widely controllable flexibility for fusion protein design. *Applied Microbiology and Biotechnology, 100*(1), 215–225. https://doi.org/10.1007/s00253-015-6985-3
[92] NeuroSnaps Inc. (2025a). OmegaFold [AI-based protein structure prediction platform]. https://neurosnap.ai/service/OmegaFold (accessed September-November 2025)
[93] Wu, R., Ding, F., Wang, R., et al. (2022). High-resolution de novo structure prediction from primary sequence using OmegaFold [Preprint]. *bioRxiv*. https://doi.org/10.1101/2022.07.21.500999
[94] NeuroSnaps Inc. (2025c). DynamicBind [AI-based ligand-specific protein-ligand complex structure prediction platform]. https://neurosnap.ai/service/DynamicBind (accessed September-Novemeber 2025)
[95] Lu, W., Zhang, J., Huang, W., Zhang, Z., Jia, X., Wang, Z., Shi, L., Li, C., Wolynes, P. G., & Zheng, S. (2025). DynamicBind: Predicting ligand-specific protein–ligand complex structure with a deep equivariant generative model. *Nature Communications, 16*(1), 1234. https://doi.org/10.1038/s41467-025-12345-y
[96] National Center for Biotechnology Information (NCBI). (2025). iCn3D: Interactive chain viewer 3D [Computer software]. National Library of Medicine. https://www.ncbi.nlm.nih.gov/Structure/icn3d/full.html (accessed September-November 2025)
[97] Wang, J., Youkharibache, P., Marchler-Bauer, A., et al. (2020). iCn3D, a web-based 3D viewer for sharing 1D/2D/3D representations of biomolecular structures. *Bioinformatics, 36*(1), 131–135. https://doi.org/10.1093/bioinformatics/btz502
[98] NeuroSnaps Inc. (2025b). IntelliFold (AlphaFold 3) [AI-based structure prediction platform]. https://neurosnap.ai/service/IntelliFold%20(AlphaFold3) (accessed September-Novemeber 2025)
[99] Jumper, J., Evans, R., Pritzel, A., Green, T., Figurnov, M., Ronneberger, O., Tunyasuvunakool, K., Bates, R., Žídek, A., Potapenko, A., Bridgland, A., Meyer, C., Kohl, S. A. A., Ballard, A. J., Cowie, A., Romera-Paredes, B., Nikolov, S., Jain, R., Adler, J., ... & Hassabis, D. (2021). Highly accurate protein structure prediction with AlphaFold. *Nature, 596*(7873), 583–589. https://doi.org/10.1038/s41586-021-03819-2
[100] D. Sehnal, S. Bittrich, M. Deshpande, R. Svobodová, K. Berka, V. Bazgier, S. Velankar, S.K. Burley, J. Koča, A.S. Rose (2021) Mol* Viewer: modern web app for 3D visualization and analysis of large biomolecular structures (2021) *Nucleic Acids Research 49*:W431-W437 https://doi.org/10.1093/nar/gkab314
[101] H.M. Berman, J. Westbrook, Z. Feng, G. Gilliland, T.N. Bhat, H. Weissig, I.N. Shindyalov, P.E. Bourne, The Protein Data Bank (2000) *Nucleic Acids Research 28*: 235-242 https://doi.org/10.1093/nar/28.1.235
[102] Luckow, V. A., Lee, S. C., Barry, G. F., & Olins, P. O. (1993). Efficient generation of infectious recombinant baculoviruses by site-specific transposon-mediated insertion of foreign genes into

a baculovirus genome propagated in Escherichia coli. *Journal of Virology, 67*(8), 4566–4579. https://doi.org/10.1128/JVI.67.8.4566-4579.1993

[103] Ruidong Wu, Fan Ding, Rui Wang, Rui Shen, Xiwen Zhang, Shitong Luo, Chenpeng Su, Zuofan Wu, Qi Xie, Bonnie Berger, Jianzhu Ma, Jian Peng. Neurosnap Inc. (2022). Neurosnap: An online platform for computational biology and chemistry. Available at: https://neurosnap.ai/ (accessed September-November 2025)

Figures

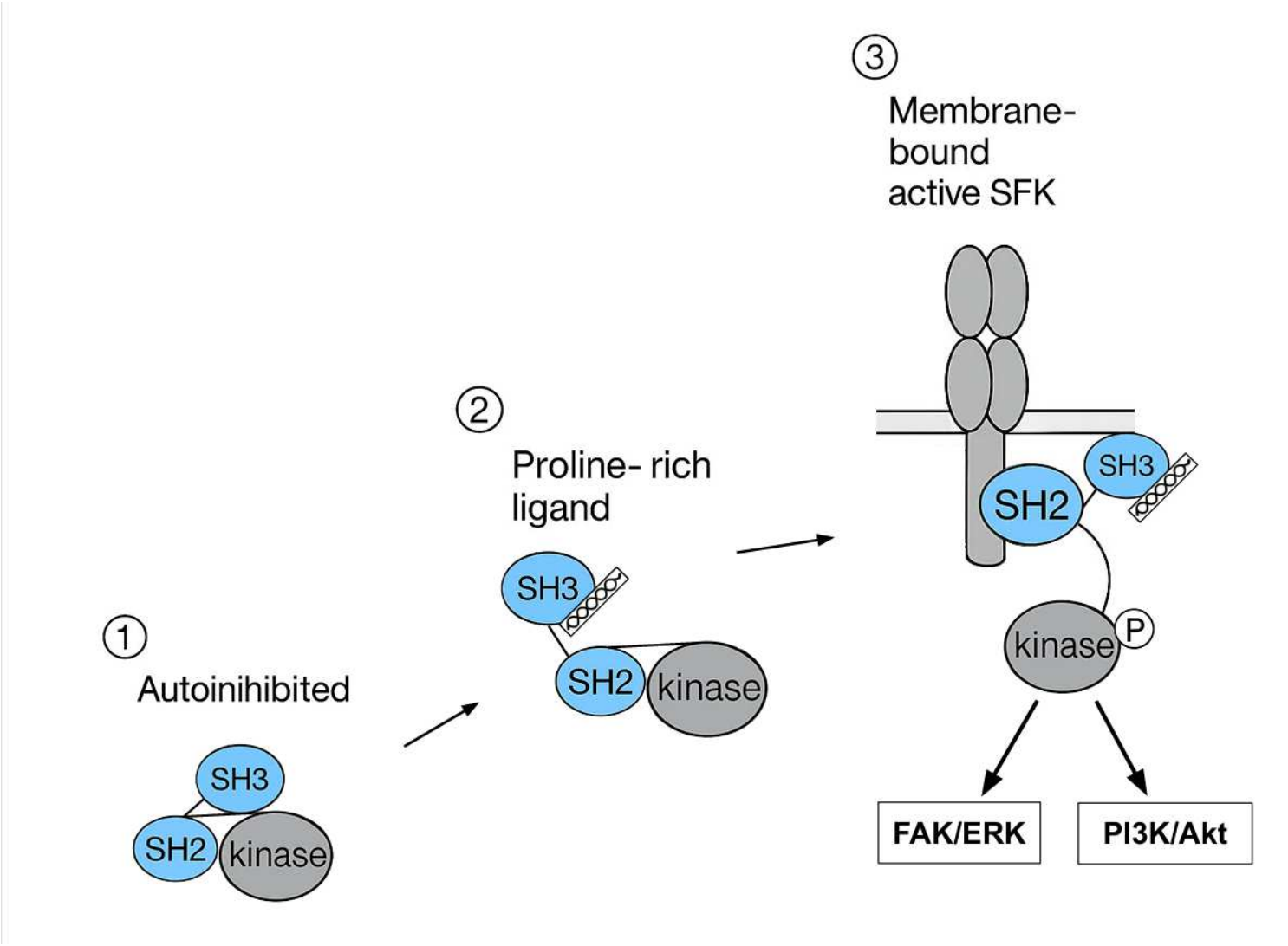

Figure 1

Figure 1. Mechanism of Src family kinase activation by proline-rich ligand. (1) Autoinhibition: In the inactive state, the SH3 domain binds the SH2–kinase linker, and the SH2 domain binds a C-terminal tail phosphotyrosine residue, keeping Src family kinases (SFKs) autoinhibited. (2) Ligand Binding: A proline-rich ligand binds to the SH3 domain, disrupting the autoinhibited conformation and allowing for SH2 domain interaction with phosphotyrosines on partially activated receptors. (3) Membrane Activation: Binding of the SH2 domain facilitates recruitment of SFKs to the membrane. Upon SH2 domain binding, autophosphorylation within the activation loop fully activates SFKs, initiating downstream signaling cascades via the focal adhesion kinase (FAK)–extracellular signal-regulated kinase (ERK) and the phosphoinositide 3-kinase (PI3K)–protein kinase B (Akt) pathways. Abbreviations: Akt, protein kinase B; ERK, extracellular signal-regulated kinase; FAK, focal adhesion kinase; PI3K, phosphoinositide 3-kinase; SFK, Src family kinase; SH2/SH3, Src homology 2/3 domains.

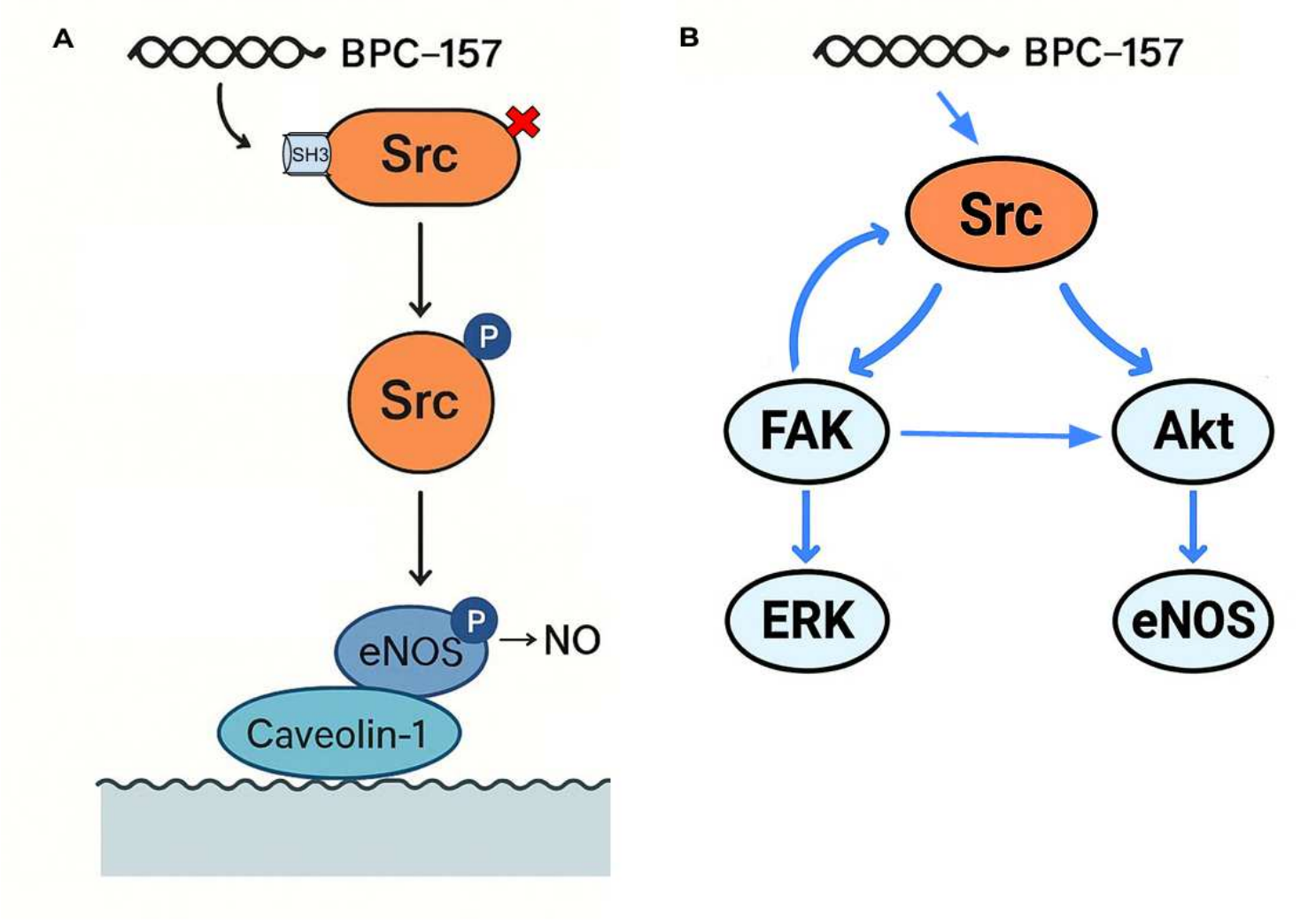

Figure 2

Figure 2. Proposed mechanism of BPC-157–induced Src activation and parallel healing pathways. (A) BPC-157 is proposed to bind the SH3 domain of Src (Src family kinases; c-Src, Fyn, and Yes), disrupting the autoinhibitory conformation and facilitating autophosphorylation of the catalytic domain. Phosphorylated Src subsequently displaces the inhibitory caveolin-1–endothelial nitric oxide synthase (eNOS) complex via direct phosphorylation of eNOS, leading to nitric oxide (NO) production. This model is based on the findings reported by Hsieh et al. [*5*]. (B) Src activation by BPC-157 triggers focal adhesion kinase (FAK) and protein kinase B (Akt) signaling pathways. FAK activation reinforces Src signaling via a positive feedback loop and promotes extracellular signal-regulated kinase (ERK) activation. Activated FAK can also initiate Akt signaling. Involvement of phosphoinositide 3-kinase is not shown. Arrows indicate activation. Abbreviations: Akt, protein kinase B; ERK, extracellular signal-regulated kinase; eNOS, endothelial nitric oxide synthase; FAK, focal adhesion kinase; NO, nitric oxide; SH3, Src homology 3 domain; Src, Src family kinase (c-Src, Fyn, and Yes)

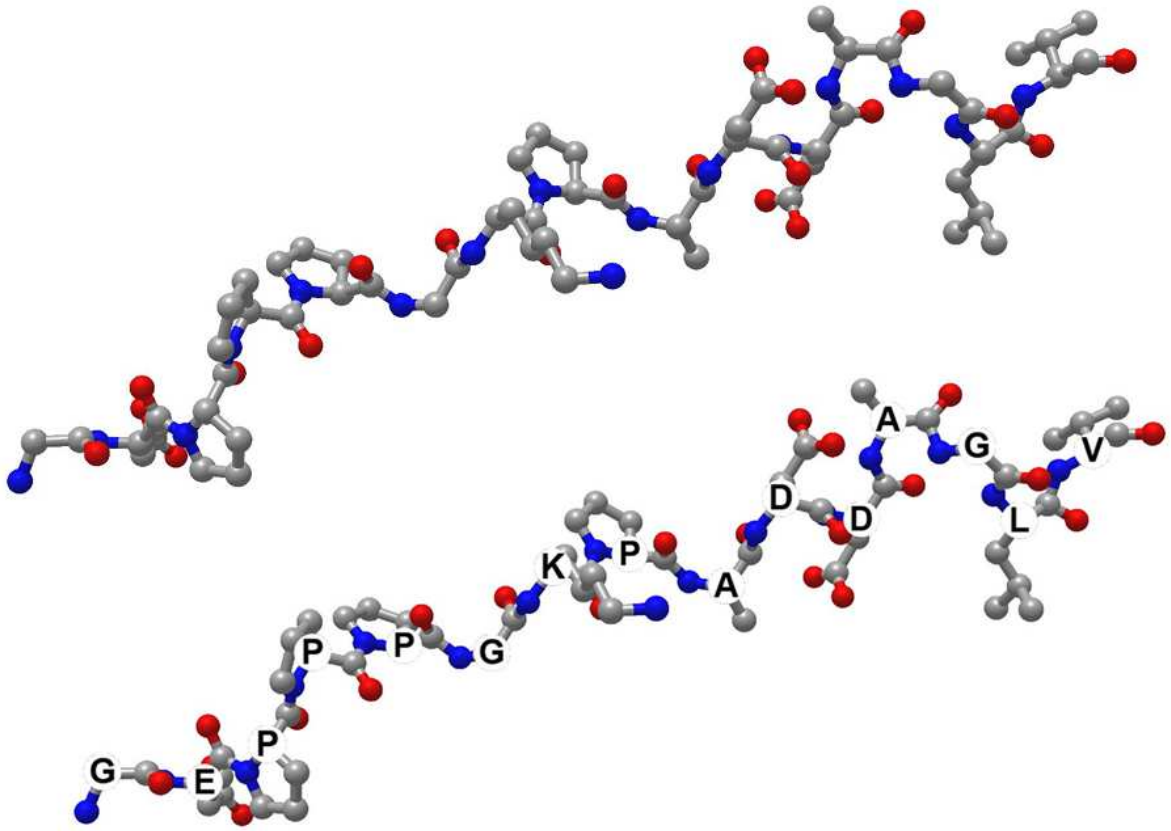

Figure 3

Figure 3. Predicted three-dimensional structure of BPC-157. (Top panel) Predicted BPC-157 tertiary structure indicating a polyproline II helix conformation. (Bottom panel) Structure annotated with the BPC-157 amino acid sequence *GEPPPGKPADDAGLV*. Atom colors are carbon (grey), oxygen (red), and nitrogen (blue).

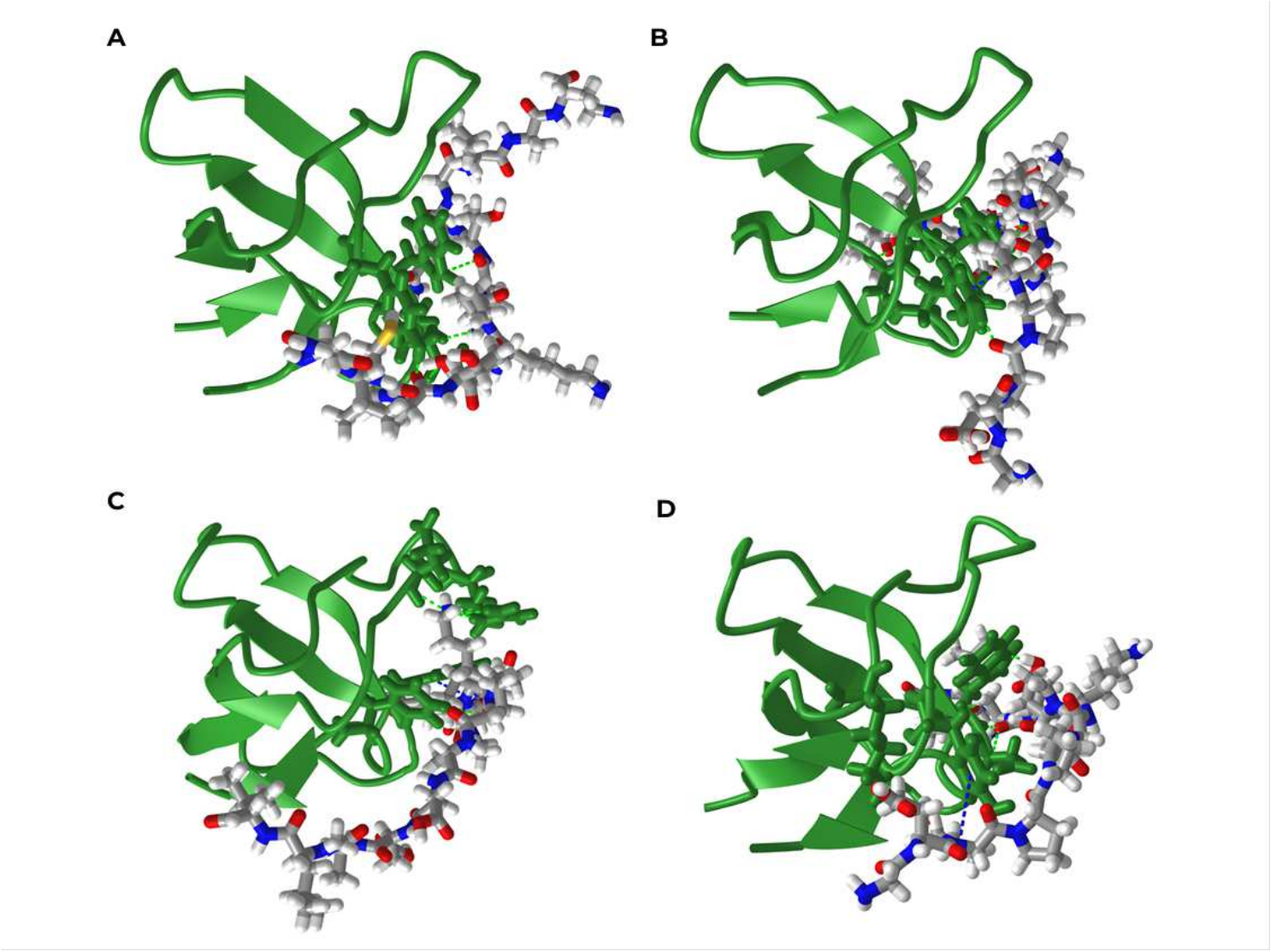

Figure 4

Figure 4. In silico docking of BPC-157 and c-Src SH2-linker peptide within SFK SH3 domain binding grooves. (A) Predicted autoinhibited conformation of c-Src SH3 domain bound to SH2-linker peptide. (B) Predicted BPC-157 binding to c-Src SH3 domain, oriented N- to C-terminus. (C) Predicted BPC-157 binding to Yes SH3 domain, oriented C- to N-terminus. (D) Predicted BPC-157 binding to Fyn SH3 domain, oriented N- to C-terminus. SH3 domains are shown as green ribbons, peptides in atom colors (carbon, grey; oxygen, red; nitrogen, blue; sulfur, yellow). Interacting SH3 residues are depicted as sticks. Dotted lines indicate predicted interactions: red, cation–π; blue, π–π stacking; green, hydrogen bonds. PDB identifiers of SH3 domains analyzed: c-Src (1SRL), Yes (2HDA), Fyn (1NYF). Abbreviation: SH3, Src homology 3 domain.

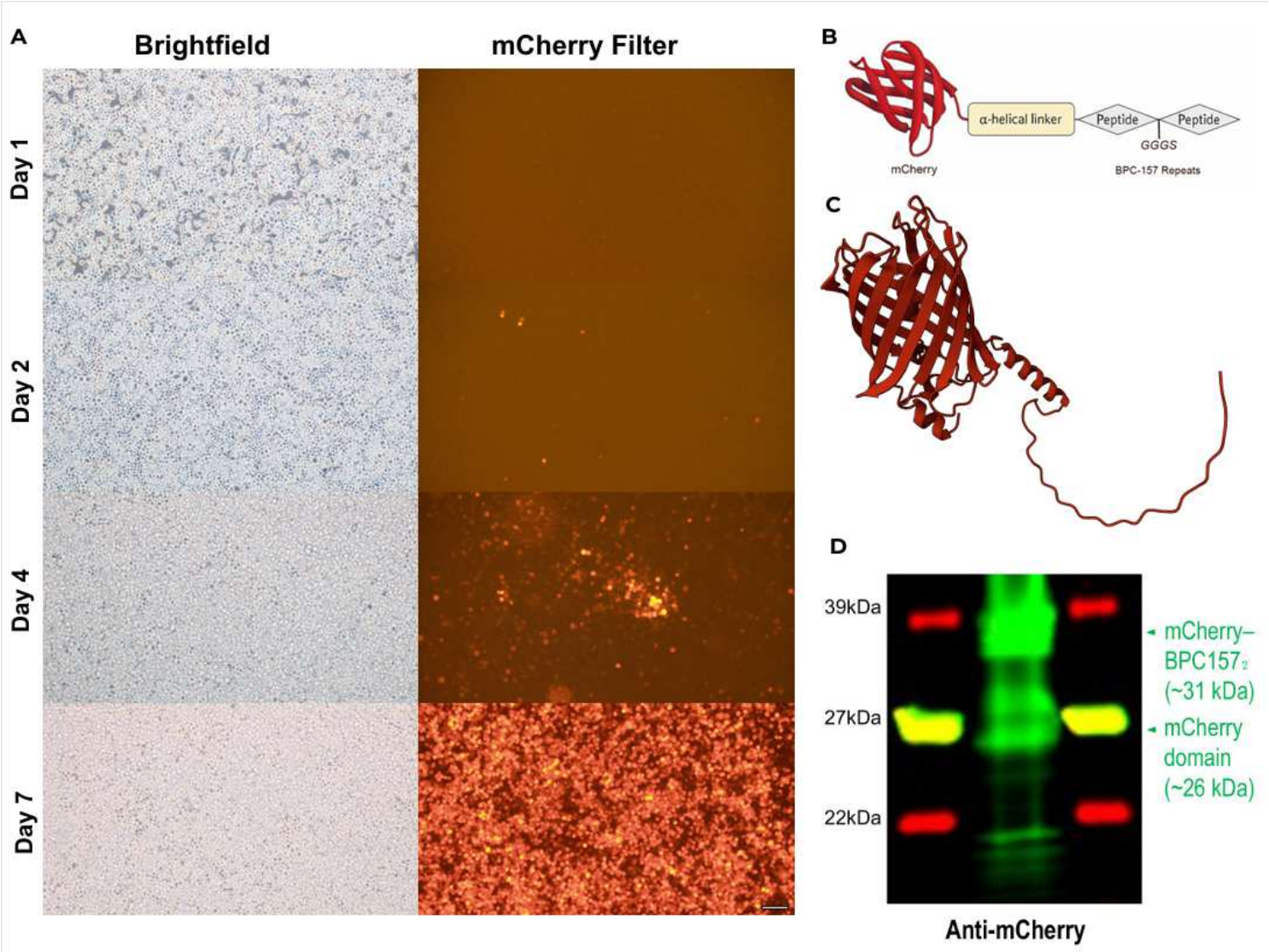

Figure 5

Figure 5. Validation of mCherry–BPC157$_2$ expression in Sf9 cells: fluorescence imaging, structural prediction, and immunoblot analysis. (A) Time course of mCherry fluorescence in Sf9 cells following baculovirus transduction. Brightfield and corresponding fluorescence images (530–550 nm Hg lamp excitation) were captured at days 1, 2, 4, and 7 post‐infection. Scale bar = 100 µm, consistent across all panels. (B) Schematic representation of the mCherry–BPC157$_2$ fusion protein. (C) Predicted 3D structure of mCherry–BPC157$_2$ generated with AlphaFold3. (D) Immunoblot of transduced Sf9 cell lysates probed with a polyclonal anti‐mCherry antibody. Lane 2 shows a band cluster at ~31–34 kDa, consistent with the predicted full‐length fusion (30.7 kDa). Higher‐migrating species correspond to ER‐processing variants retaining the N‐terminal secretory sequence (33.1 kDa) and putative post‐translationally modified forms. Additional bands at ~29 kDa (single‐tail mCherry–BPC157) and ~26.6 kDa (mCherry domain) indicate truncated fragments. Prestained molecular weight markers (22, 27, 39 kDa) are shown in Lanes 1 and 3. Abbreviation: Sf9, *Spodoptera frugiperda* cells.

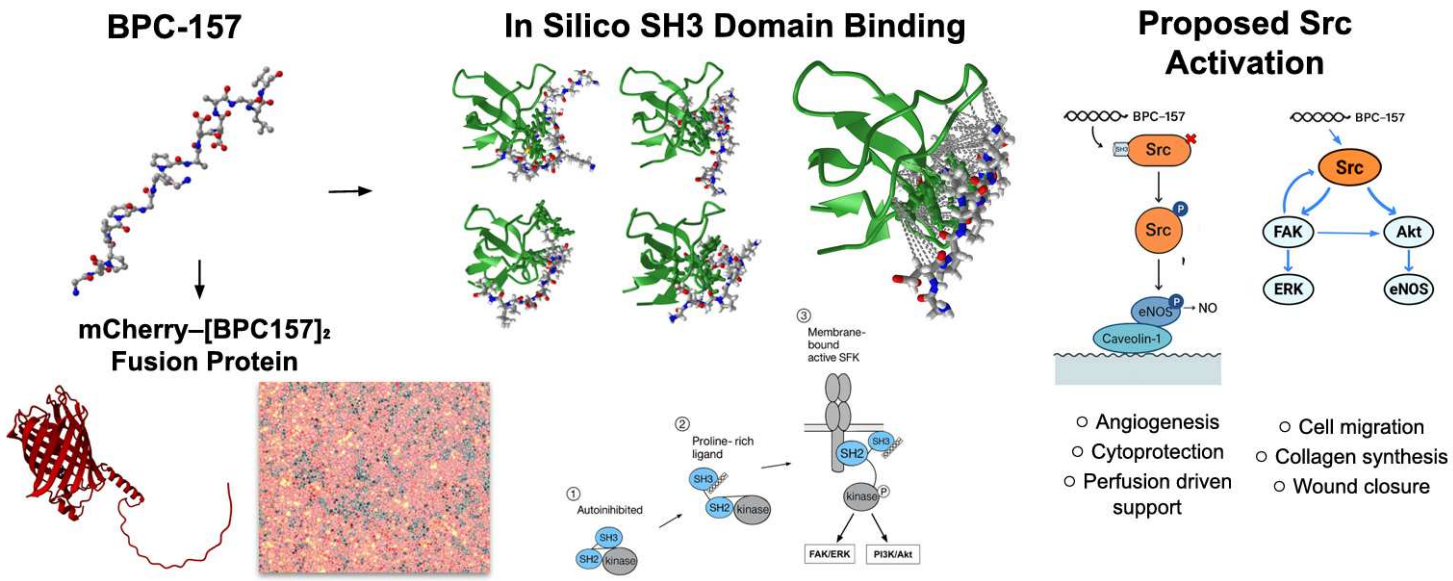

Figure 6

BPC-157 Binding to SH3 Domains and Activation of Src Family Kinases: In Silico Modeling and Fluorescent Fusion Protein Production

Supplementary Files

This is a list of supplementary files associated with this preprint. Click to download.

- SupplementaryFilesBPC157BindingtoSH3DomainsSchlosser2025Final.zip